Supplementary Information

Combination of Nanoparticles with Single-Metal Sites Synergistically Boosts Co-Catalyzed Formic Acid Dehydrogenation

Yanzhe Shi[1,6], Bingcheng Luo[2,6], Rui Sang[3], Dandan Cui[4], Ye Sun[1,7], Runqi Liu[1], Zili Zhang[5], Yifei Sun[1,7], Henrik Junge[3], Matthias Beller[3,7], and Xiang Li[1,7]

[1] *School of Energy and Power Engineering, Beihang University, Beijing, 100191, P.R. China.*

[2] *College of Science, China Agricultural University, Beijing 100083, P.R. China.*

[3] *Leibniz-Institut für Katalyse, Albert-Einstein-Straße 29a, 18059, Rostock, Germany.*

[4] *School of Physics, Beihang University, Beijing, 100191, P.R. China.*

[5] *School of Science, China University of Geosciences, Beijing 100083, P.R. China.*

This file includes:

Supplementary Methods

Supplementary Notes 1 and Supplementary Notes 2

Supplementary Figures: Figure S1-S47

Supplementary Tables: Table S1-S15

Supplementary Reference

[6] These authors contributed equally: Yanzhe Shi, Bingcheng Luo.

[7] Corresponding author's E-mail address: suny@buaa.edu.cn (Y. Sun). sunif@buaa.edu.cn (Y. Sun). Matthias.Beller@catalysis.de (M. Beller). xiangli@buaa.edu.cn (X. Li).

Table of Contents

1 Supplementary Methods

1.1 Chemicals

DCOOH (95 wt.% in H_2O, 99 atom% D) and HCOOD (95 wt.% in D_2O, 98 atom% D) were purchased from CDN Isotopes, Canada. DCOOD (95 wt. % in D_2O, 98 atom% D) was purchased from Aladdin, China.

1.2 Preparation of control Co SAs catalysts with CoN_2C_2 units

We refer to previous studies to synthesize control Co SAs catalyst with CoN_2C_2 units.[1] Firstly, $Zn(NO_3)_2 \cdot 6H_2O$ (1.116 g) and 3.5 mmol of $Co(NO_3)_2 \cdot 6H_2O$ (0.546 g) were mixed and dissolved in 30 mL of methanol. Then, 2-methylimidazole (1.232 g) was dissolved in 30 ml of methanol and added to the above solution. The mixture was stirred at room temperature for 24 hours. Finally, the product was separated by centrifugation at 6429 g for 10 min and washed thoroughly three times with methanol. The resulting powder was dried overnight at 60 °C under vacuum before use. The dried powder of ZnCo-BMOF was pyrolyzed in a tube furnace at 800 °C for 1 hour, 900 °C for 1 hour and 1000 °C for 1 hour under an argon flow at a heating rate of 5°C min^{-1}. Then, the sample was cooled to room temperature.

1.3 Preparation of control Co NPs catalysts

We refer to previous studies to synthesize control Co NPs catalysts.[1] The synthesis of Co-ZIF-67 is identical to that of ZnCo-BMOF except for the addition of $Zn(NO_3)_2$-$6H_2O$. Firstly, $Co(NO_3)_2 \cdot 6H_2O$ (0.546 g) were dissolved in 30 mL of methanol. Then, 2-methylimidazole (1.232 g) were dissolved in 30 mL of methanol and added to the above solution. The mixture was stirred at room temperature for 24 hours. Finally, the product was separated by centrifugation at 6429 g for 10 min and washed thoroughly three times with methanol. The resulting powder was dried overnight at

60 °C under vacuum before use. Then, the dried powder of Co-ZIF-67 was pyrolyzed in a tube furnace at 800 °C for 1 hour, 900 °C for 1 hour and 1000 °C for 1 hour under an argon flow at a heating rate of 5°C min^{-1}. Then, it was cooled to room temperature.[1]

2 Supplementary Note 1

2.1 HAADF-STEM

High-angle annular dark-field scanning transmission electron microscopy (HAADF-STEM) experiments were performed using FEI Titan G2 and FEI Titan Themis Z microscope equipped with a probe and image corrector, a four segment DF4 detector. The HAADF-STEM has a convergence angle of 25 mrad and a collection angle of 50 -200 mrad. The probe current for the EELS experiment was 30 pA, using a collection angle of approximately 100 mrad, with an exposure time of 0.03 s per pixel and a dispersion of 0.6 eV per channel. EDS elemental mapping images were also obtained on the FEI Titan Themis Z microscope.

2.2 X-ray photoelectron spectroscopy (XPS)

An X-ray photoelectron spectrometer (Thermo Fisher model ESCALAB 250Xi) was used for the respective measurements. The vacuum of the chamber was 8×10^{-10} Pa, the excitation source was Al ka-rays (E=1486.6 eV), the operating voltage was 14.7 kV, the filament current was 16 mA, and the signal was accumulated for 5 cycles. The test flux energy (Passing-Energy) was 100 ev for the full spectrum, 30 eV for the narrow spectrum, 0.05 eV step, 50 ms dwell time, and charge correction with C 1s=284.80 eV binding energy standard.

2.3 X-ray absorption fine structure (XAFS)

The XANES and EXAFS of Co K-edge spectra are collected by Table XAFS-500 (Specreation Instruments Co.,

Ltd. China). The beamline utilizes a Si/Ge monochromator crystal with an SDD detector behind the focusing position of the KB mirror for transmission and fluorescence mode X-ray absorption spectroscopy. The photon flux on the sample is in the range of $1x10^6 \sim 2x10^6$ photons/sec for X-ray energy is 4.5-20 kV. Athena (version 0.9.26) was used to process background, pre-edge line, and post-edge line calibrations. Then, Fourier transformed fitting was processed in Artemis (version 0.9.26). Wavelet Transform analysis was carried out by importing the $\chi(k)$ exported from Athena into the Hama Fortran code.

3 Supplementary Note 2

3.1 Product gas composition analysis

The outlet gas content was determined by gas chromatography (6890A, Agilent Technologies):

GC a): HP -AL/S / FID – hydrocarbons, Carboxen / TCD - permanent gases, Ar carrier gas.

GC b): MolSieve 13X/ TCD / MTN-1 Methanizer for FID CO analysis / FID - permanent gases, Ar carrier gas.

The different gas contents were calibrated using standard gas mixtures with the following volume percentages:

GC a): H_2: 5%, 10%, 15%, 20%, 25%, 50%, 100%

CO_2: 5%, 10%, 15%, 20%, 25%, 50%, 100%

b): CO: 10 ppm, 100 ppm, 250 ppm, 1000 ppm

GC analysis provides the relative composition of the different components of the collected gas. The amounts of H_2, CO_2 and CO are determined, and their ratios are also established.

3.2 Calculation of gas production rate

a. The gas production rate was calculated by equation **(S1)**:

$$\text{Gas production rate} = \frac{V_{gas}}{m_{cat} \times t} \quad \textbf{(S1)}$$

b. The gas production rate based on Co was calculated by equation **(S2):**

$$\text{Gas production rate}=\frac{V_{gas}}{m_{cat}\times \text{Co (wt\%)}\times t} \quad \textbf{(S2)}$$

where V_{gas} is the gas volume corrected by blank volume, and m_{cat} is the weight of the catalyst, respectively.

c. The turnover frequency (TOF) was calculated by equation **(S3)**:

$$\text{TOF}=\frac{\frac{V'_{gas}}{(V_{m,H_2,25℃}+V_{m,CO_2,25℃})}}{n_{cat}\times t} \quad \textbf{(S3)}$$

where TOF is initial turnover frequency, V'_{gas} is the generated volume of mixture gas during the first 10 min of the reaction, n_{cat} is the mole number of the Co, and t is the reaction time.

d. The calculation of $V_{m,H_2,25℃}$ and $V_{m,CO_2,25℃}$ were carried out using equation **(S3)** and **(S4)**:

$$V_{m,H_2,25℃}=\frac{RT}{p}+b-\frac{a}{RT}=24.48\ \frac{L}{mol} \quad \textbf{(S4)}$$

$$V_{m,CO_2,25℃}=\frac{RT}{p}+b-\frac{a}{RT}=24.36\ \frac{L}{mol} \quad \textbf{(S5)}$$

where:

R: 8.3145 $m^3\cdot Pa\cdot mol^{-1}\cdot K^{-1}$;

T: 298.15 K;

P: 101325 Pa;

a (H_2): $24.7\cdot10^{-3}\cdot Pa\cdot m^6\cdot mol^{-2}$ and a (CO_2): $36.5\cdot10^{-2}\cdot Pa\cdot m^6\cdot mol^{-2}$;

b (H_2): $26.6\cdot10^{-6}\ m^3\cdot mol^{-1}$ and b (CO_2): $42.7\cdot10^{-6}\ m^3\cdot mol^{-1}$.

e. The selectivity of catalytic reactions was calculated by equation **(S6):**

$$H_2\ \text{Selectivity}=\frac{V_{H2}}{V_{CO}+V_{H2}} \quad \textbf{(S6)}$$

where V_{CO} and V_{H2} are the gas volumes of CO and H_2 produced, respectively.

4 Supplementary Figures

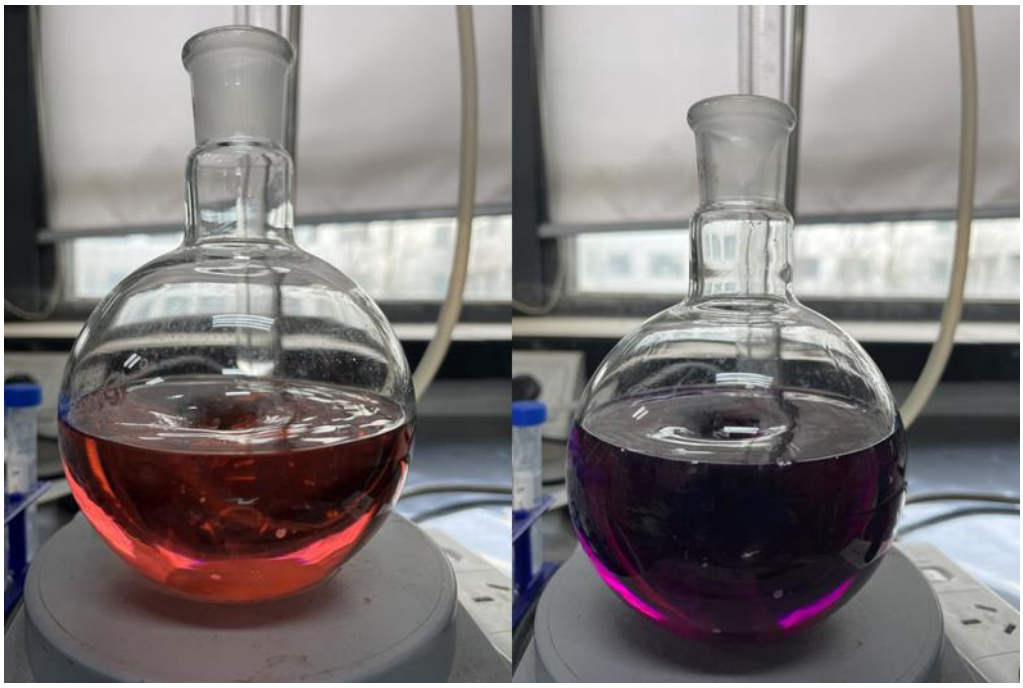

Figure S1. Photographs of the reaction mixtures before (left) and after (right) the addition of 2-methylimidazole.

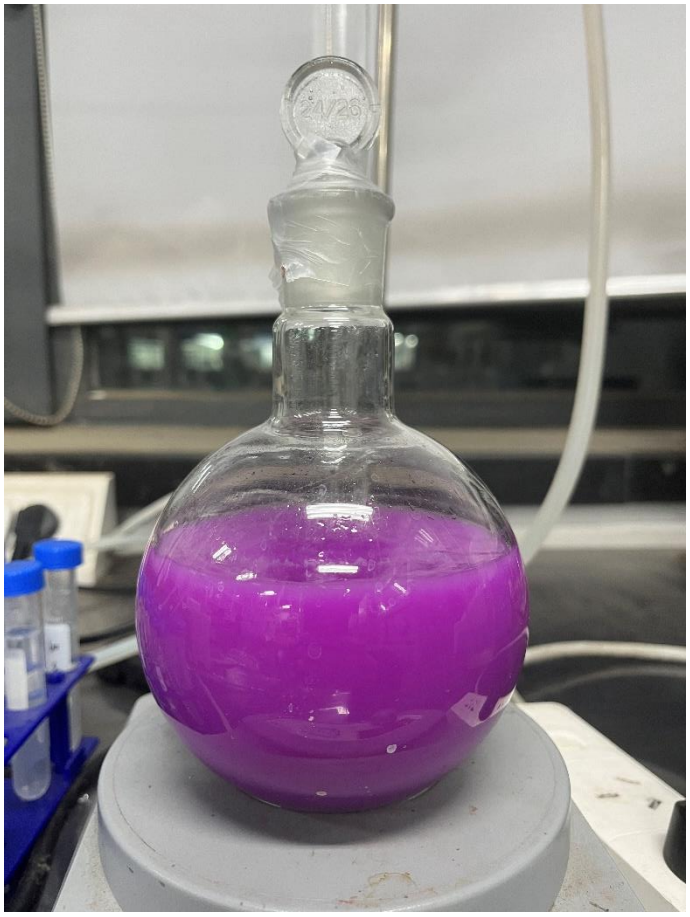

Figure S2. Photograph of the reaction mixture after 24 h of mixing.

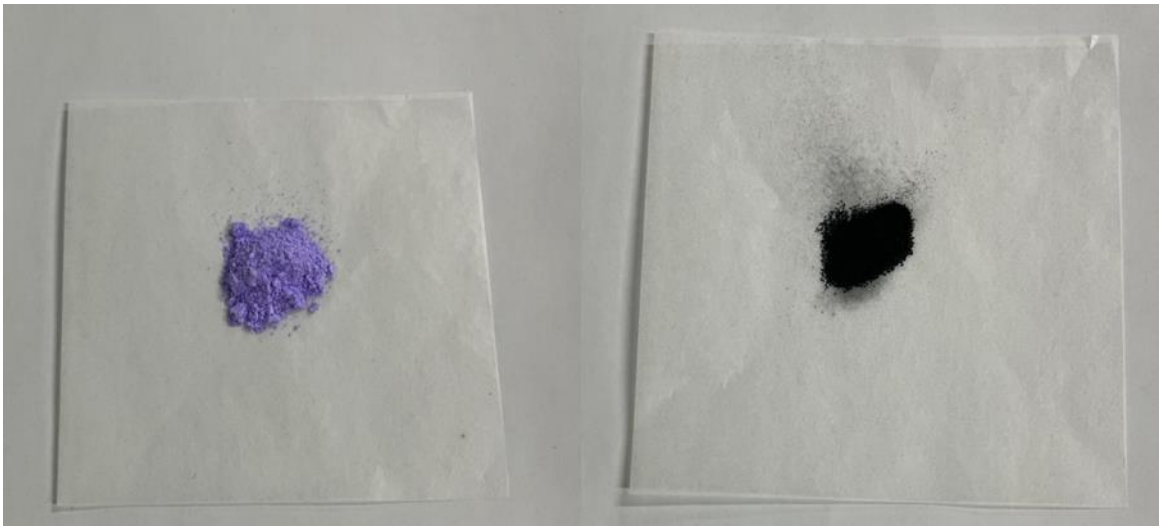

Figure S3. Photos of the (pre-)catalyst mixture before (left) and after (right) pyrolysis.

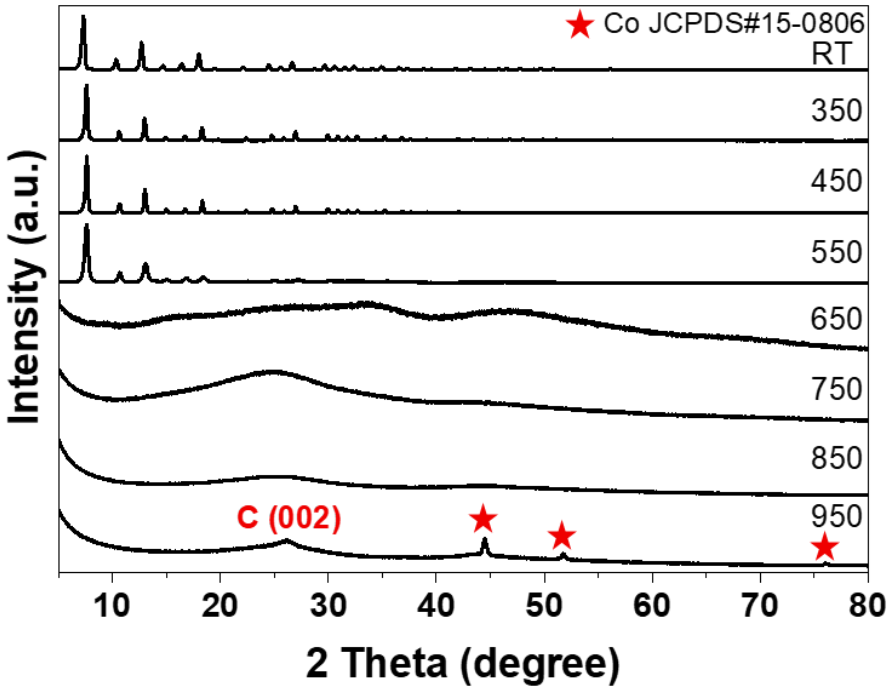

Figure S4. VTXRD spectra of CoZn-ZIF with pyrolysis temperatures ranging from room temperature to 950 ℃.

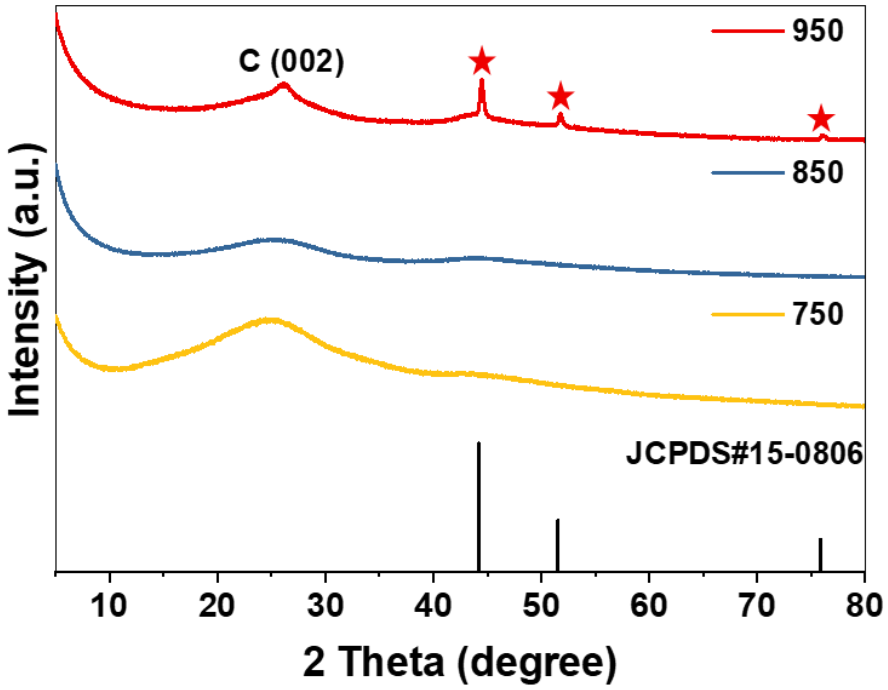

Figure S5. XRD spectra of Co-SAs/NPs@NC-950, Co-SAs/NPs@NC-850 and Co-SAs/NPs@NC-750.

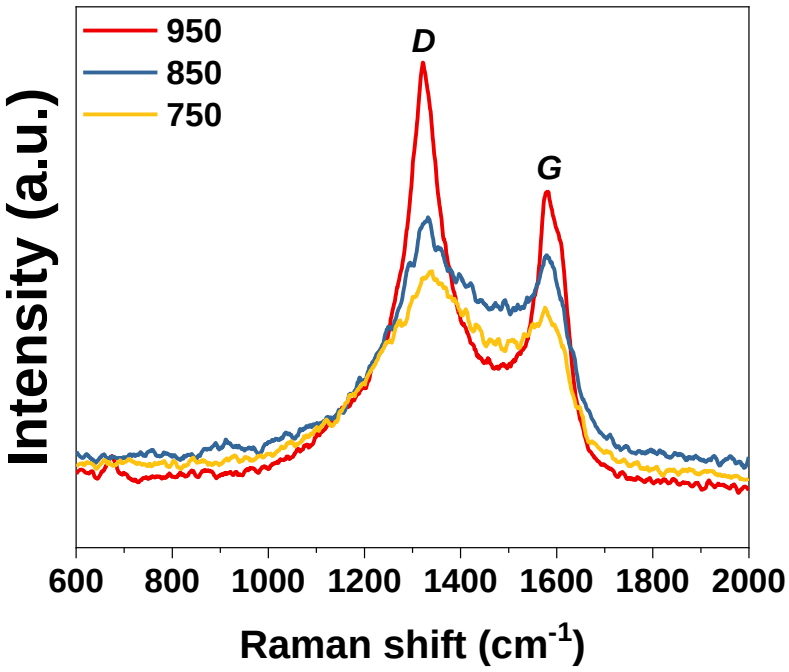

Figure S6. Raman spectra of Co-SAs/NPs@NC-950, Co-SAs/NPs@NC-850 and Co-SAs/NPs@NC-750.

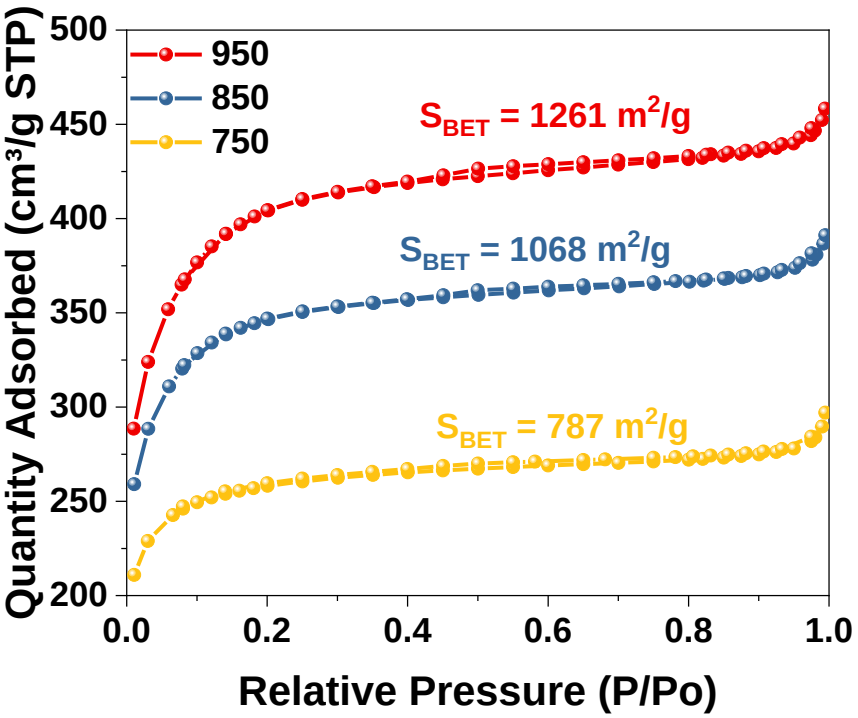

Figure S7. N_2 Adsorption isotherm of Co-SAs/NPs@NC-950, Co-SAs/NPs@NC-850 and Co-SAs/NPs@NC-750.

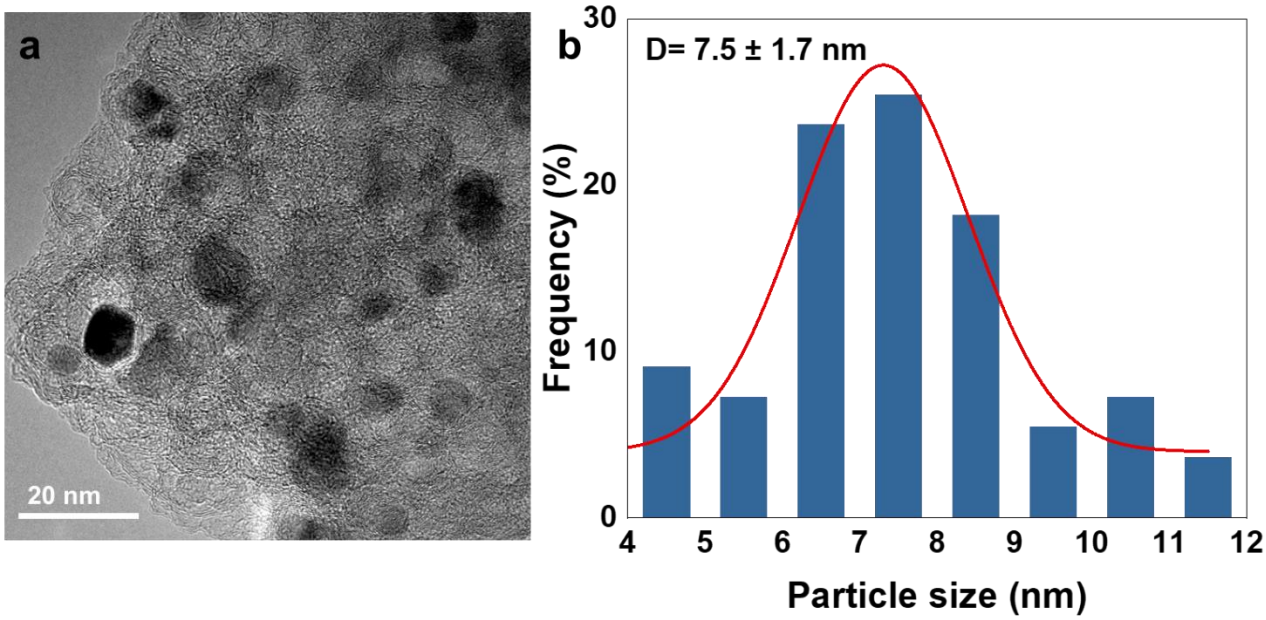

Figure S8. a TEM image and **b** the corresponding particle-size distribution histogram of Co-SAs/NPs@NC-950.

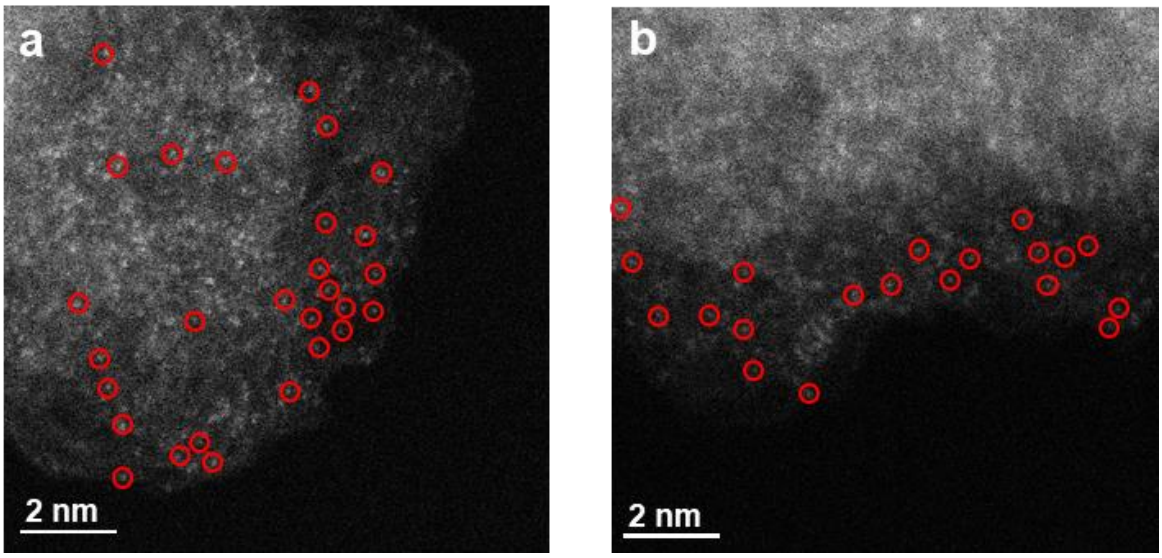

Figure S9. The HAADF-STEM image of **a** Co-SAs/NPs@NC-850 and **b** Co-SAs/NPs@NC-750 with a resolution of 2 nm.

The Co single atoms are marked with red circles.

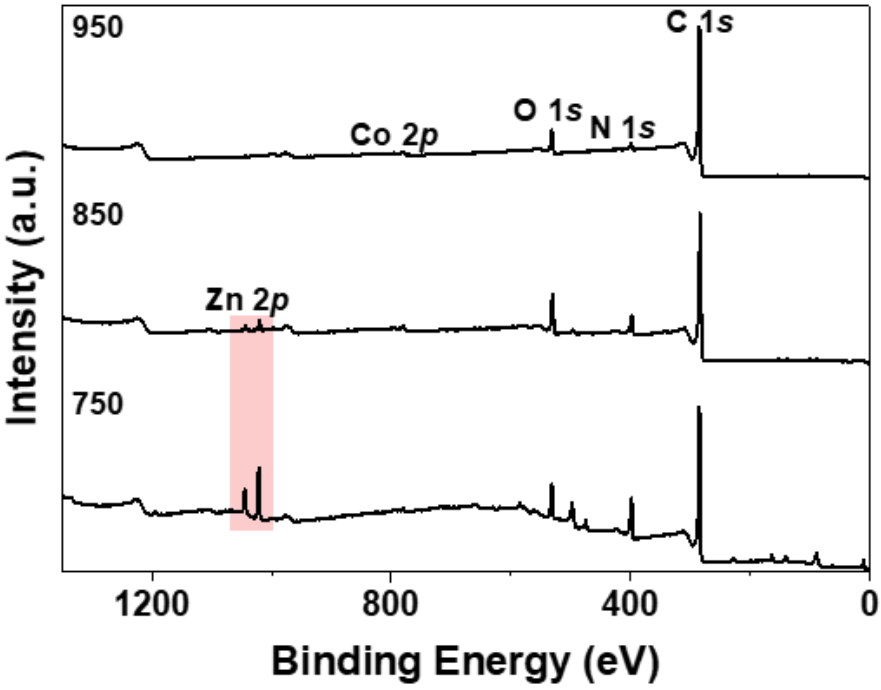

Figure S10. XPS survey scanning of Co-SAs/NPs@NC-950, Co-SAs/NPs@NC-850 and Co-SAs/NPs@NC-750.

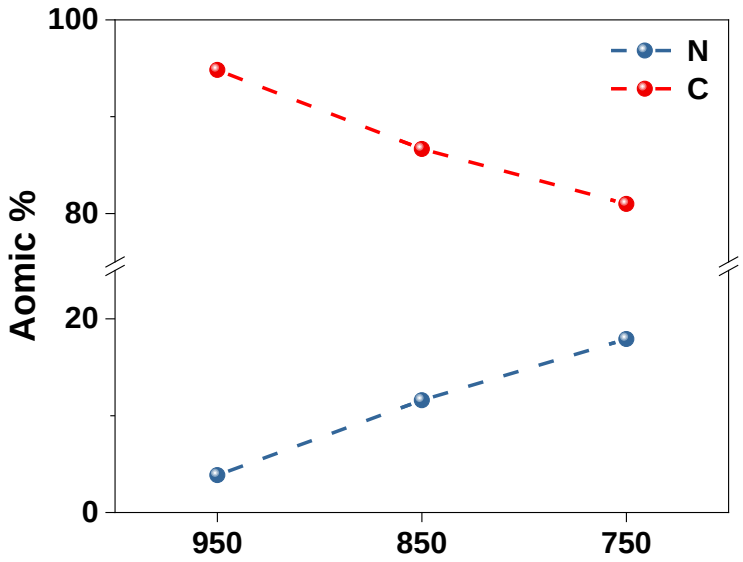

Figure S11. Atomic content of N and C for Co-SAs/NPs@NC-950, Co-SAs/NPs@NC-850 and Co-SAs/NPs@NC-750.

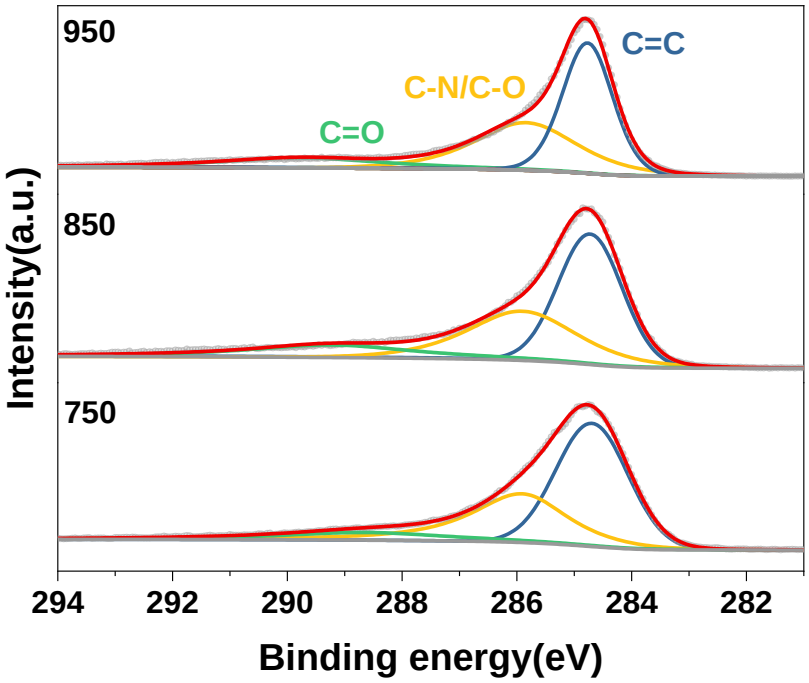

Figure S12. High-resolution XPS spectra of C 1*s* of Co-SAs/NPs@NC-950, Co-SAs/NPs@NC-850 and Co-SAs/NPs@NC-750.

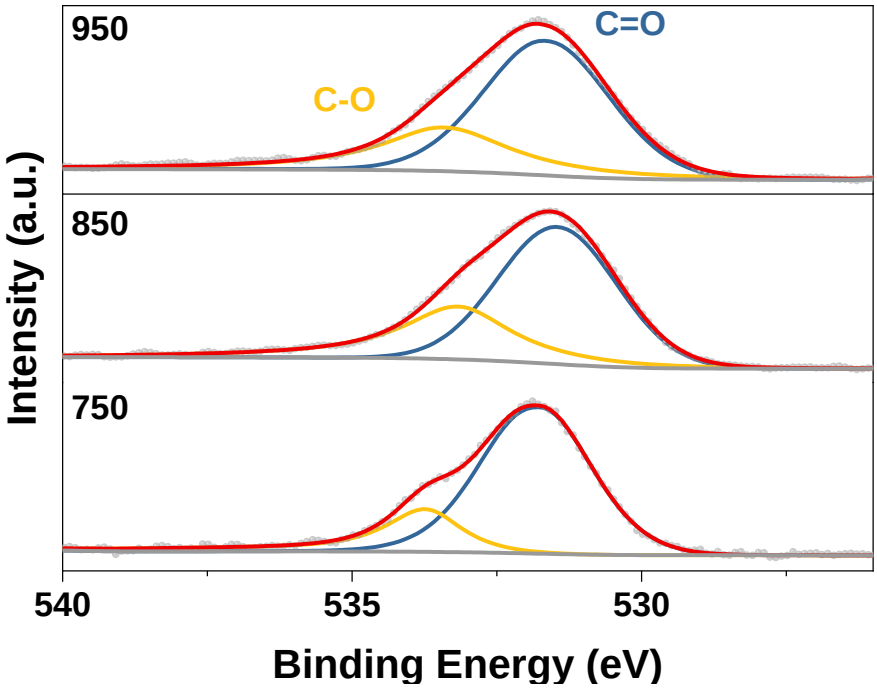

Figure S13. XPS spectra of O 1*s* of Co-SAs/NPs@NC-950, Co-SAs/NPs@NC-850 and Co-SAs/NPs@NC-750.

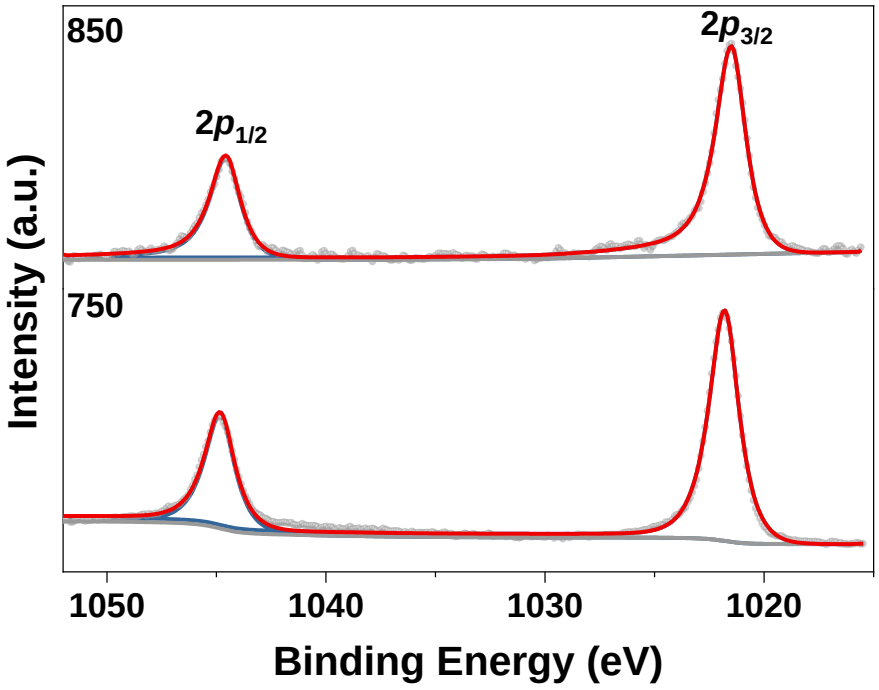

Figure S14. XPS spectra of Zn 2*p* of Co-SAs/NPs@NC-850 and Co-SAs/NPs@NC-750.

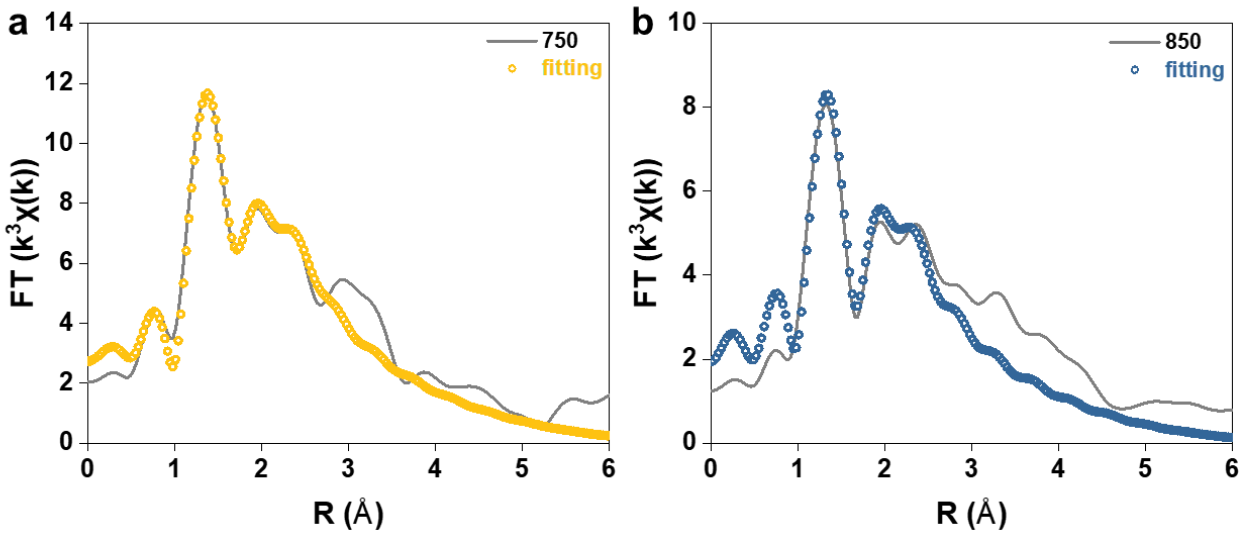

Figure S15. Corresponding Co K-edge EXAFS fitting curves of **a** Co-SAs/NPs@NC-850 and **b** Co-SAs/NPs@NC-750 in R space.

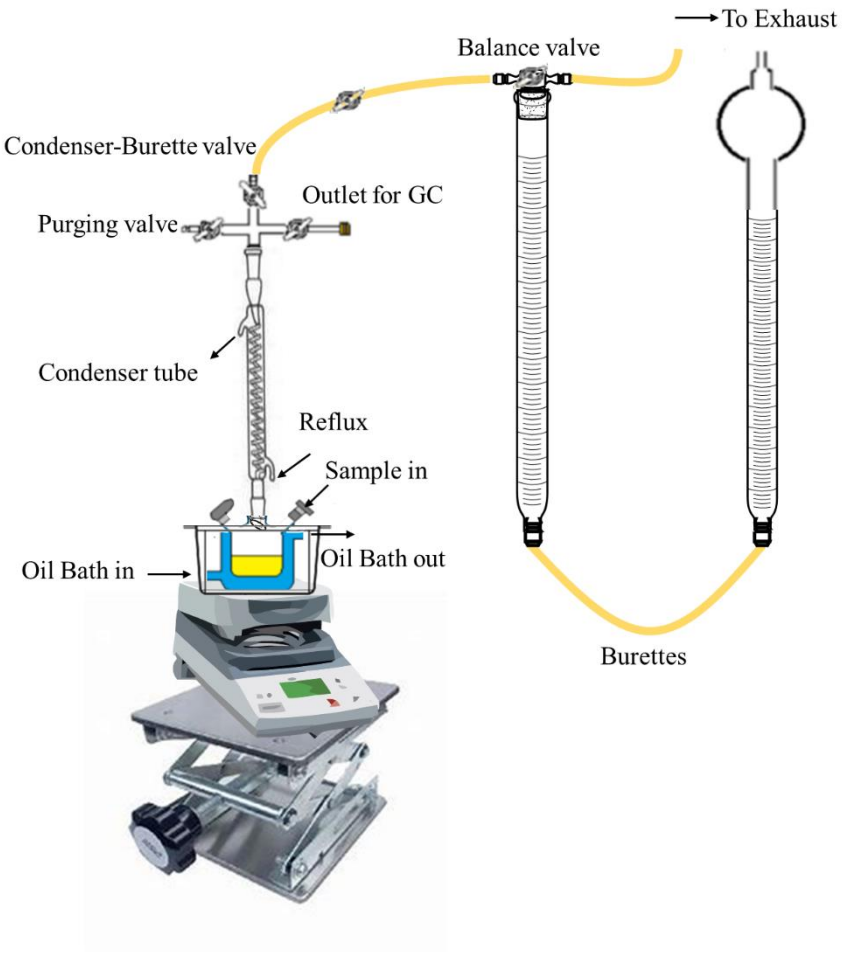

Figure S16. Experimental set-up for dehydrogenation of HCOOH.

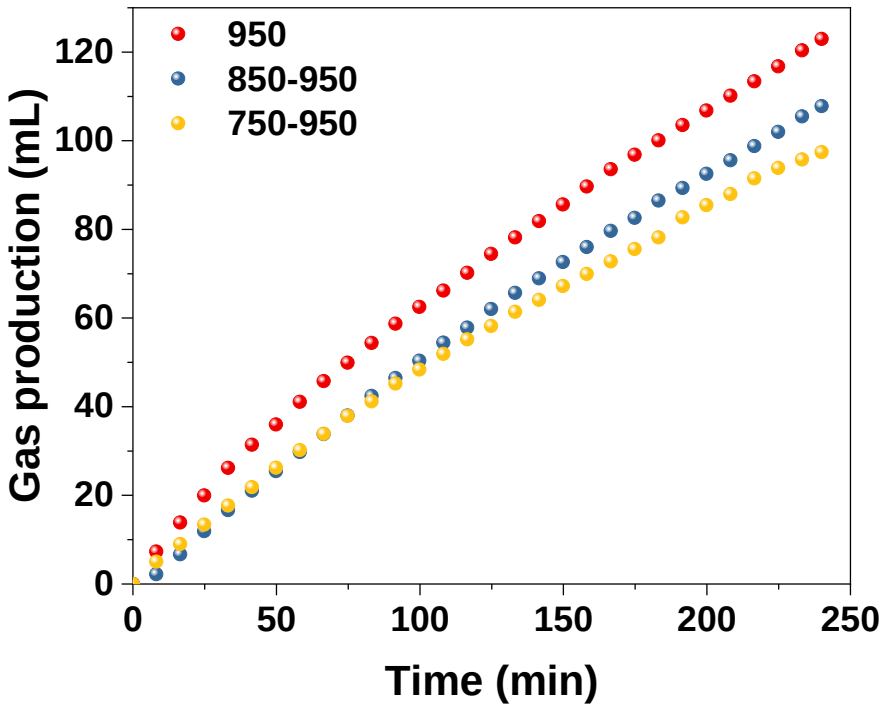

Figure S17. Plot of volume of produced gas versus time for the dehydrogenation of FA applying Co-SAs/NPs@NC-950, Co-SAs/NPs@NC-850 and Co-SAs/NPs@NC-750 after heating at 950 °C.

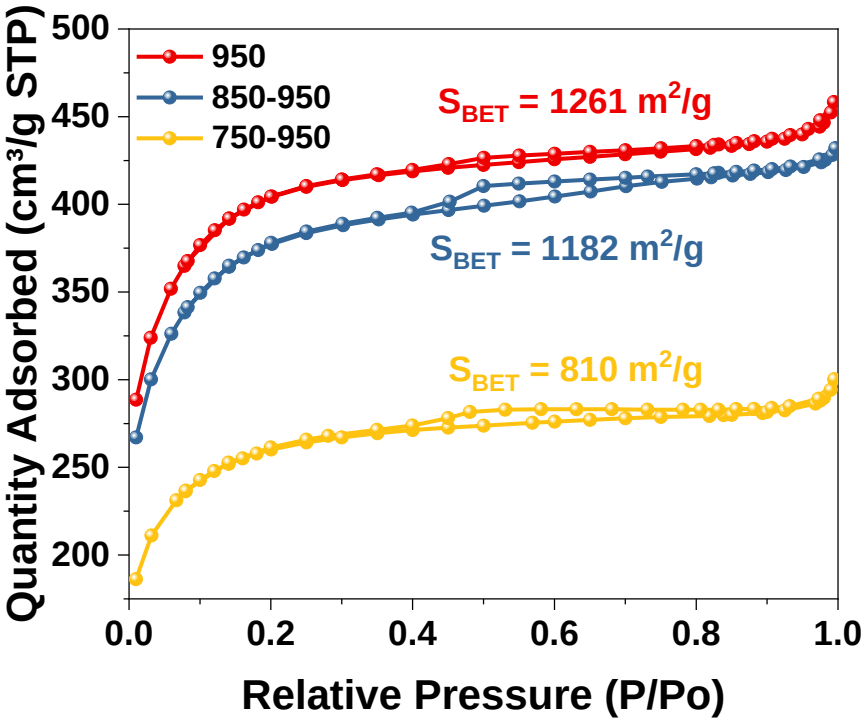

Figure S18. N_2 Adsorption isotherm of Co-SAs/NPs@NC-950, Co-SAs/NPs@NC-850 and Co-SAs/NPs@NC-750 after heating at 950 °C.

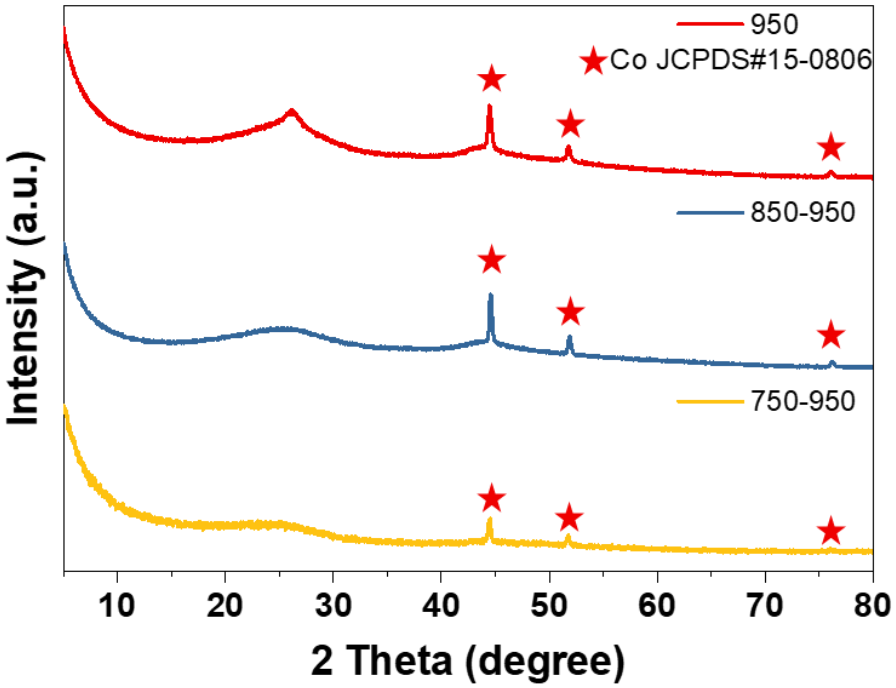

Figure S19. XRD spectra of Co-SAs/NPs@NC-950, Co-SAs/NPs@NC-850 and Co-SAs/NPs@NC-750 after heating at 950 °C.

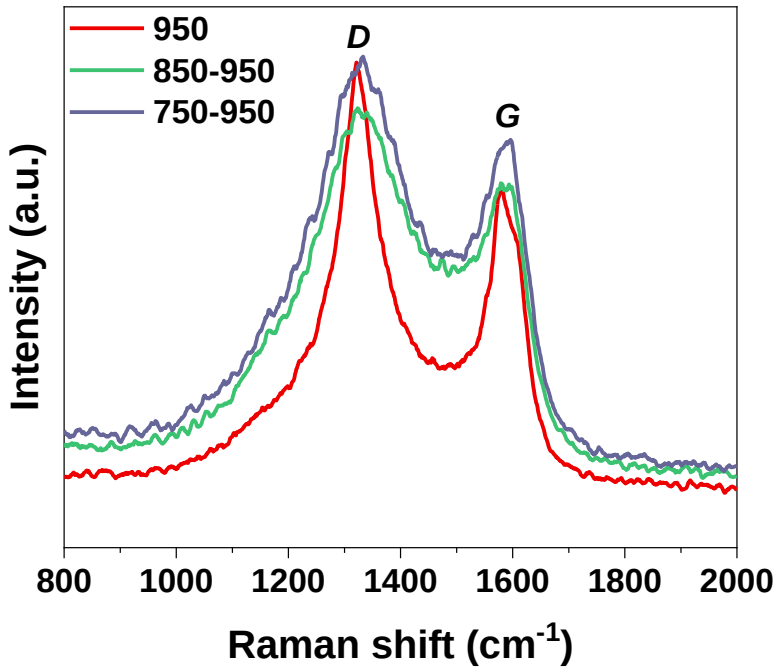

Figure S20. Raman spectra of Co-SAs/NPs@NC-950, Co-SAs/NPs@NC-850 and Co-SAs/NPs@NC-750 after heating at 950 °C.

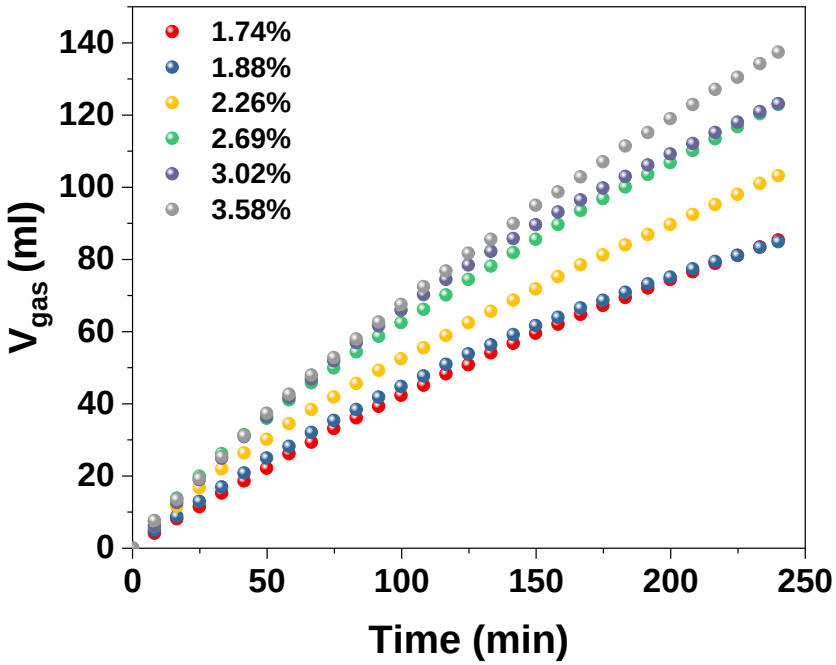

Figure S21. Plot of volume of produced gas versus time for the dehydrogenation of FA applying Co-SAs/NPs@NC-950 with different cobalt content.

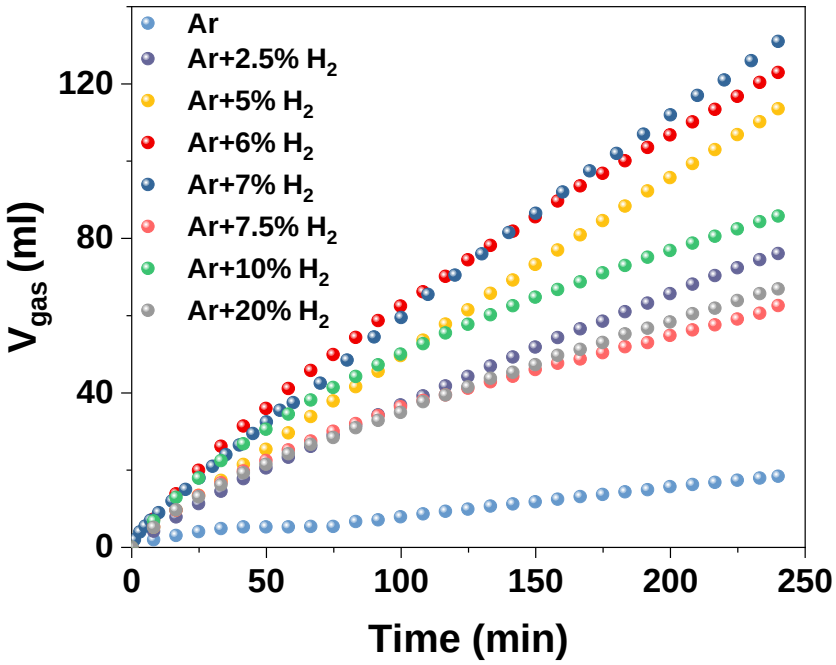

Figure S22. Plots of the volume of gas formed from FA versus time using Co-SAs/NPs@NC-950 prepared under different pyrolysis atmospheres.

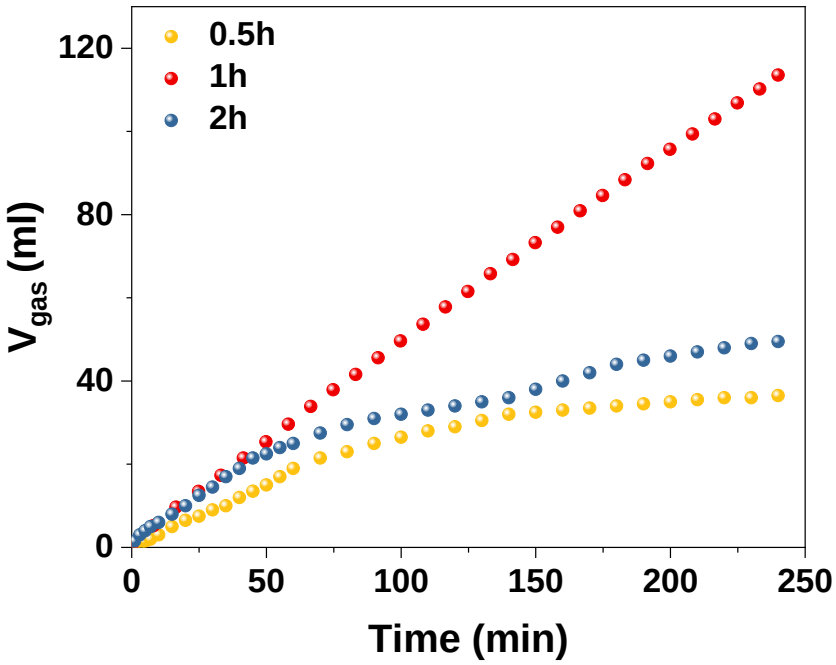

Figure S23. Plots of the volume of gas formed from FA versus time using Co-SAs/NPs@NC-950 prepared with different pyrolysis times.

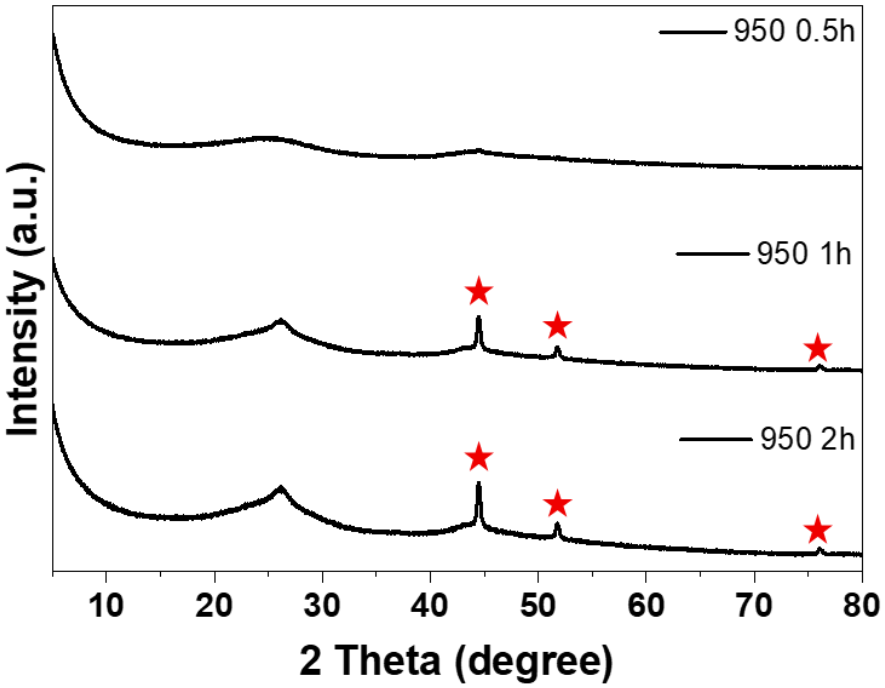

Figure S24. XRD spectra of Co-SAs/NPs@NC-950-1h, Co-SAs/NPs@NC-950-0.5h and Co-SAs/NPs@NC-950-2h.

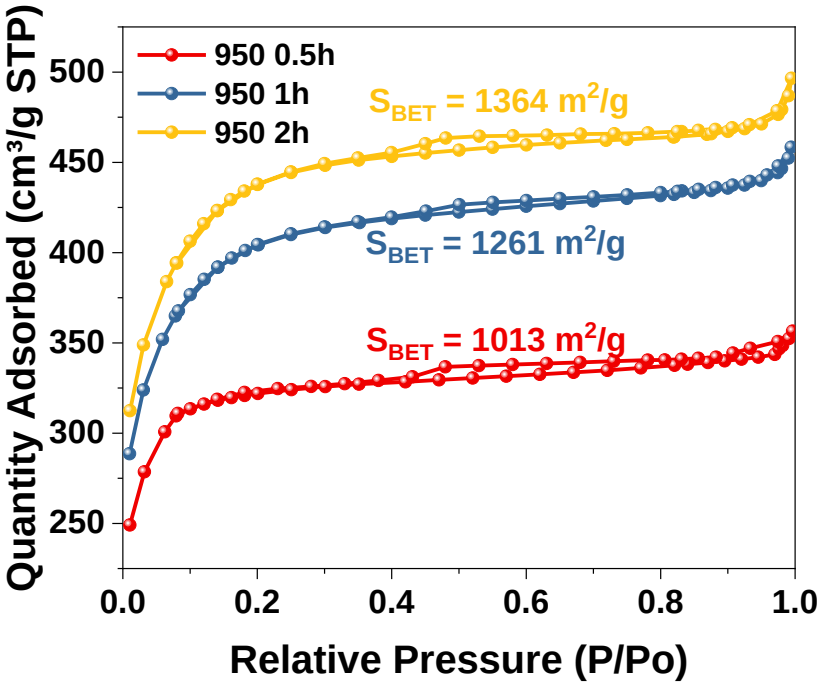

Figure S25. N_2 Adsorption isotherm of Co-SAs/NPs@NC-950-1h, Co-SAs/NPs@NC-950-0.5h and Co-SAs/NPs@NC-950-2h.

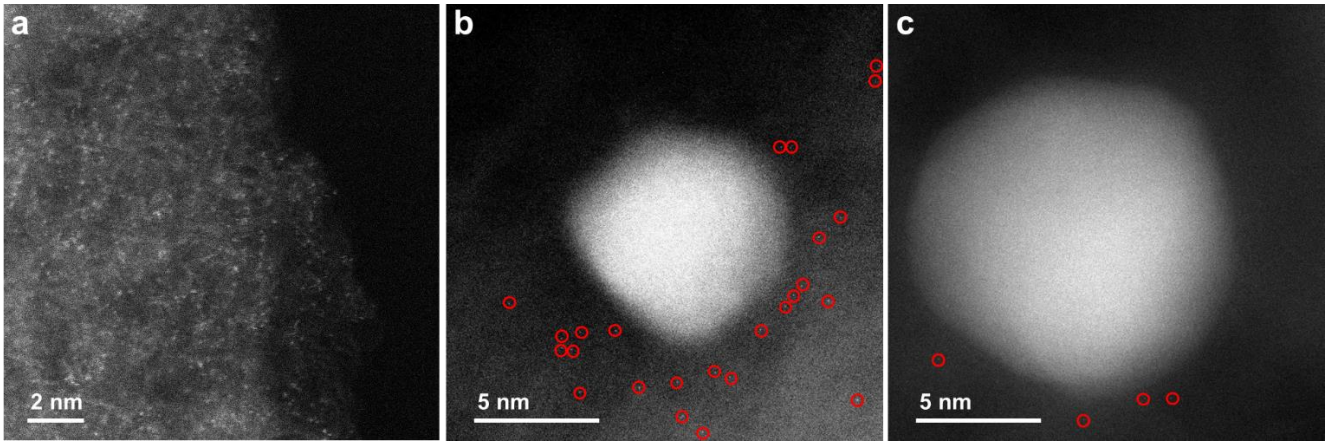

Figure S26. HAADF-STEM image of Co-SAs/NPs@NC-950-0.5h, Co-SAs/NPs@NC-950-1h and Co-SAs/NPs@NC-950-2h. Cobalt single atoms are marked with red circles.

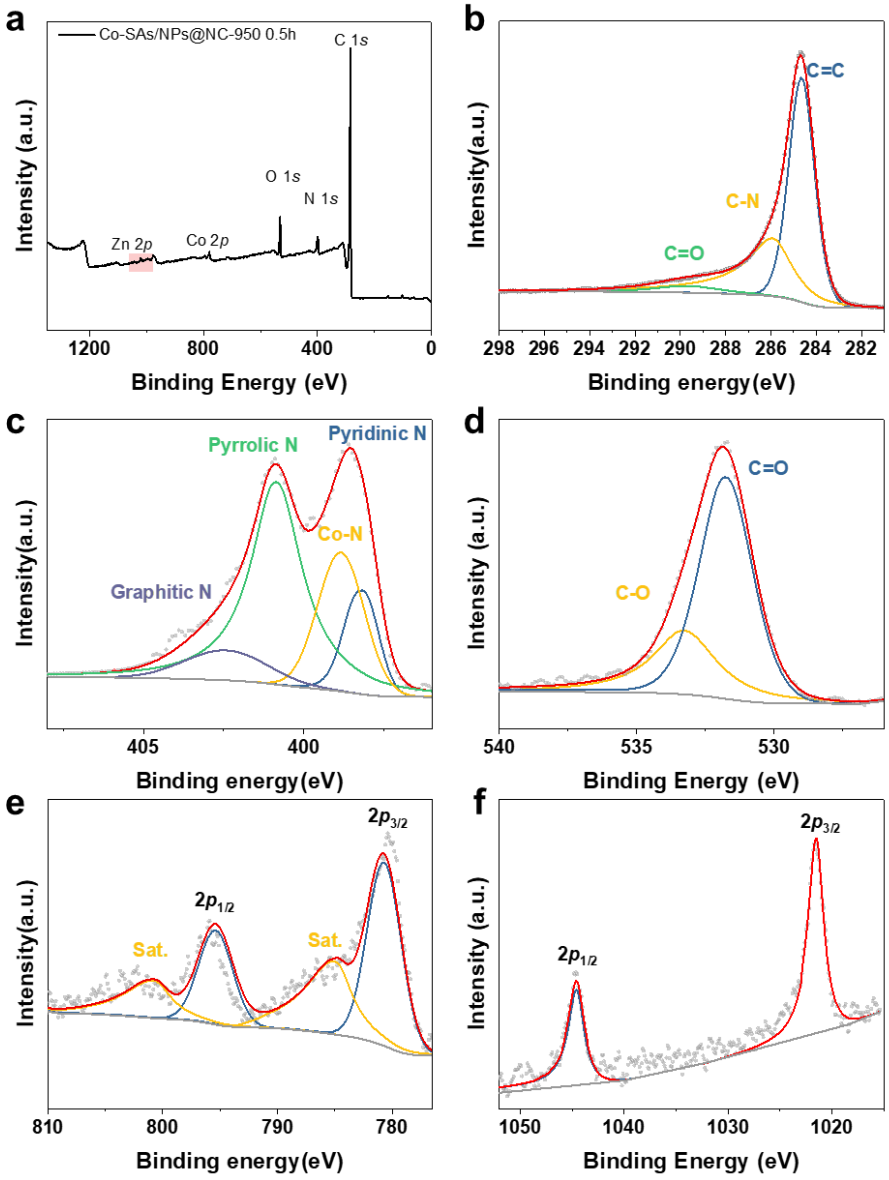

Figure S27. a XPS survey scanning. **b** C 1*s*. **c** N 1*s*. **d** O 1*s*. **e** Co 2*p*. and **f** Zn 2*p* spectra of Co-SAs/NPs@NC-950-0.5h.

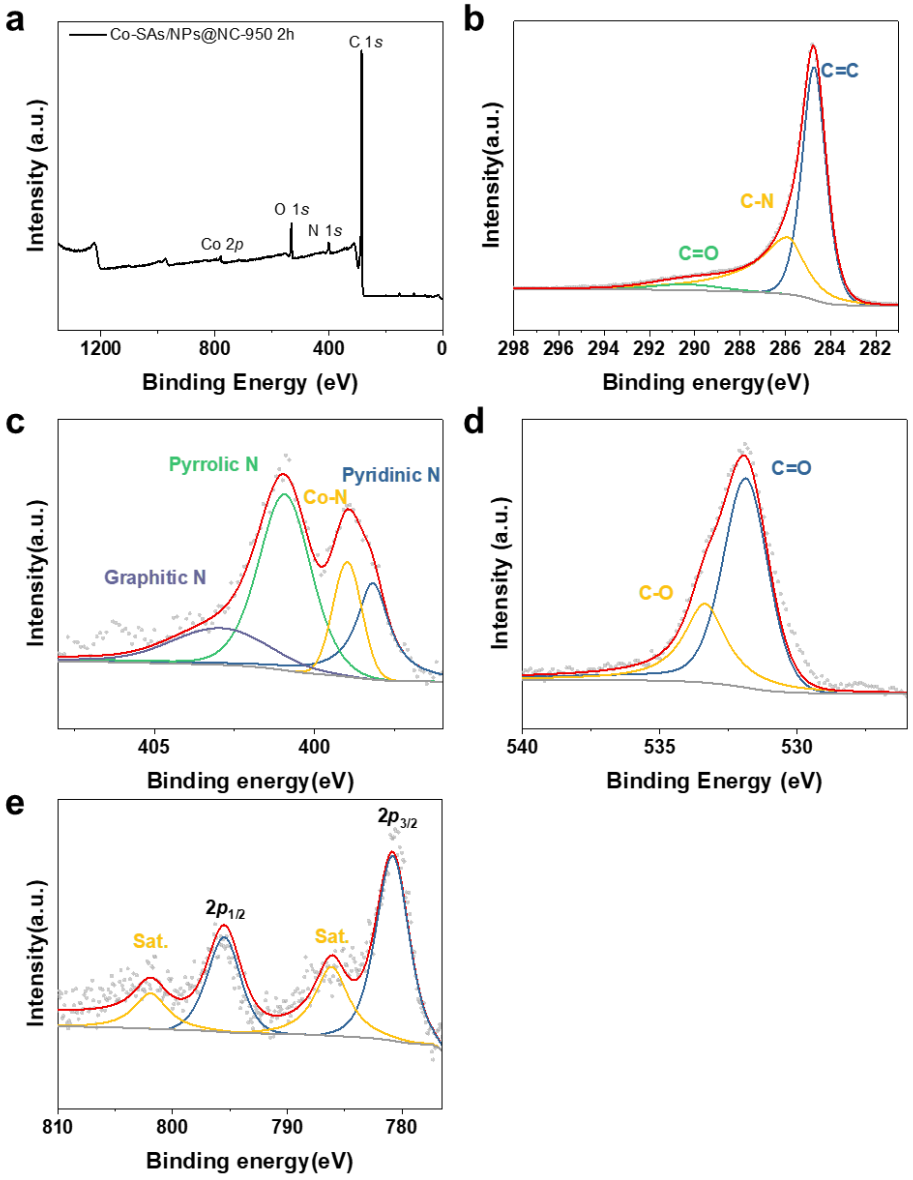

Figure S28. a XPS survey scanning. **b** C 1*s*. **c** N 1*s*. **d** O 1*s*. and **e** Co 2*p* spectra of Co-SAs/NPs@NC-950-2h.

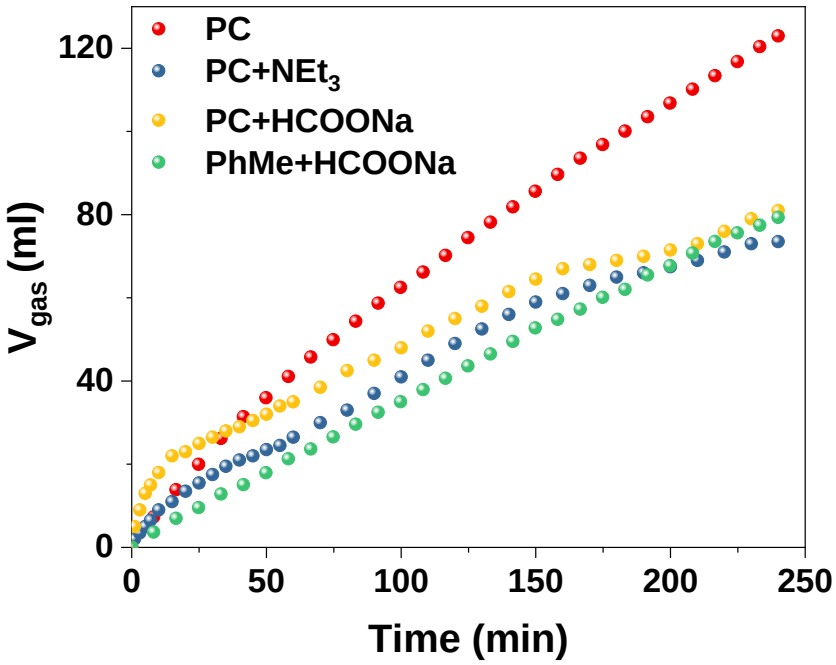

Figure S29. Plots of the volume of gas formed from FA versus time in the presence of different additives. Reaction conditions: FA (10 mmol, 377 μL), additive (1.0 mmol), Co-SAs/NPs@NC-950 (30 mg) in specified solvents (6 mL), T_{set}: 110 °C, T_{actual}: 98 °C, 4 h.

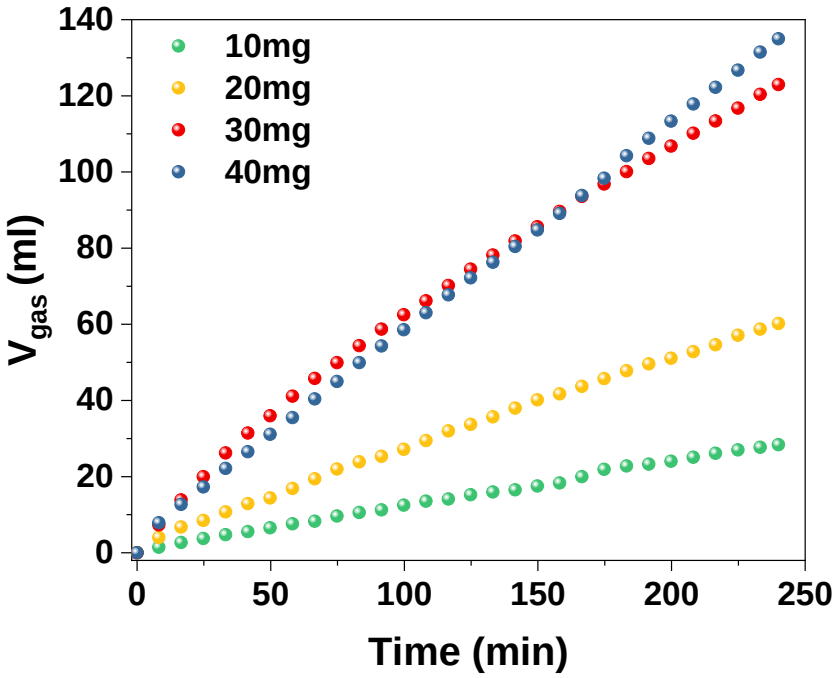

Figure S30. Plots of the volume of gas formed from FA versus time using different amounts of Co-SAs/NPs@NC-950.

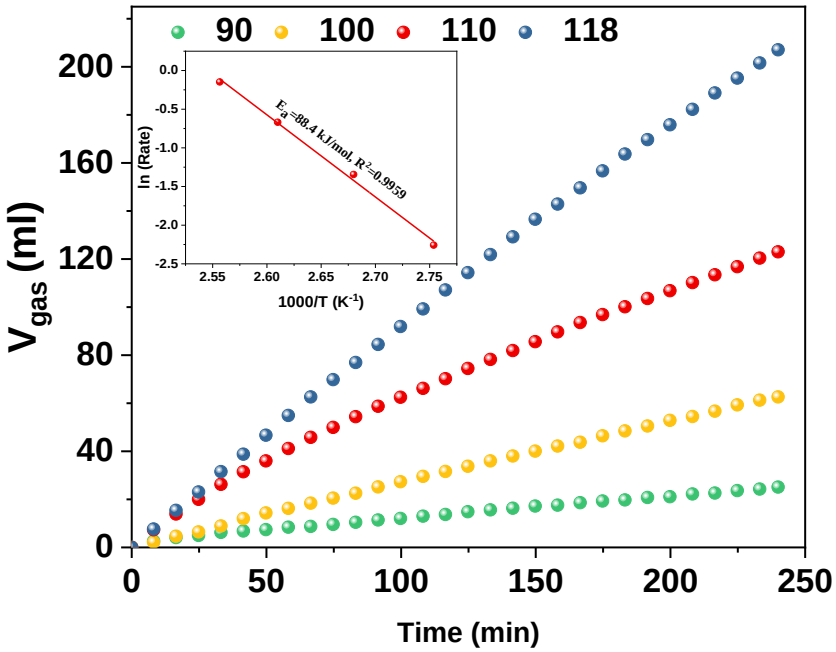

Figure S31. Formic acid dehydrogenation activity in the presence of Co-SAs/NPs@NC-950 at different temperatures, inset shows reaction activation energy.

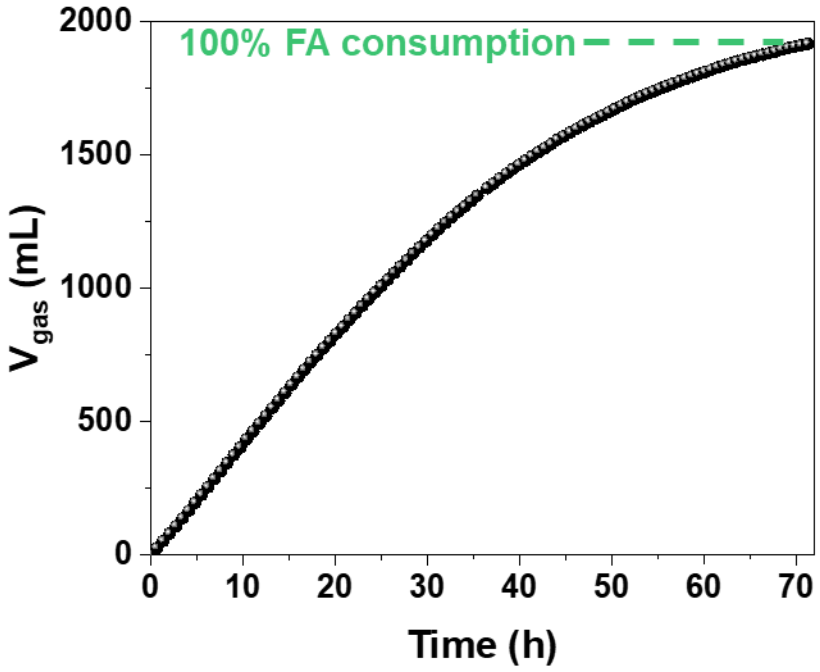

Figure S32. Long-term experiment using Co-SAs/NPs@NC-950. We observed that the actual gas production was slightly higher than the theoretical gas production, which is attributed to the blank volume (1709 mL).

General procedure:

Under an Ar atmosphere, PC (21 mL) and Co-SAs/NPs@NC-950 (30 mg) were added to a 50 mL three-neck glass reactor equipped with a magnetic stir bar. Then, the reaction solution was heated to 98 °C. After that, formic acid (35 mmol, 1.32 mL) was added. The reaction was performed at the set temperature for 72 h. The generated gas was collected by a manual burette to get the gas volume. The gas was analyzed by GC.

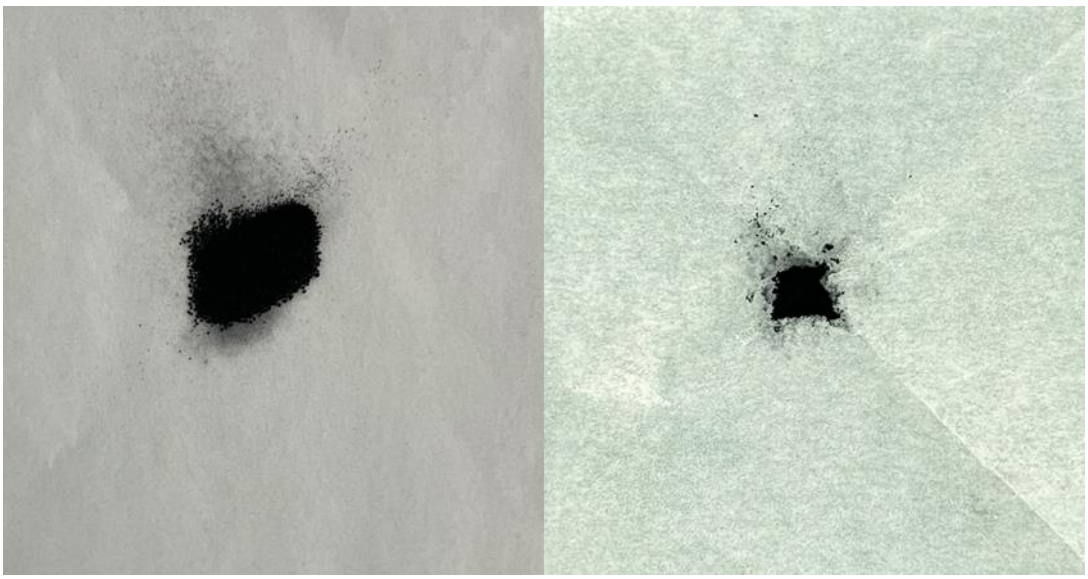

Figure S33. Fresh and used Co-SAs/NPs@NC-950 samples**.**

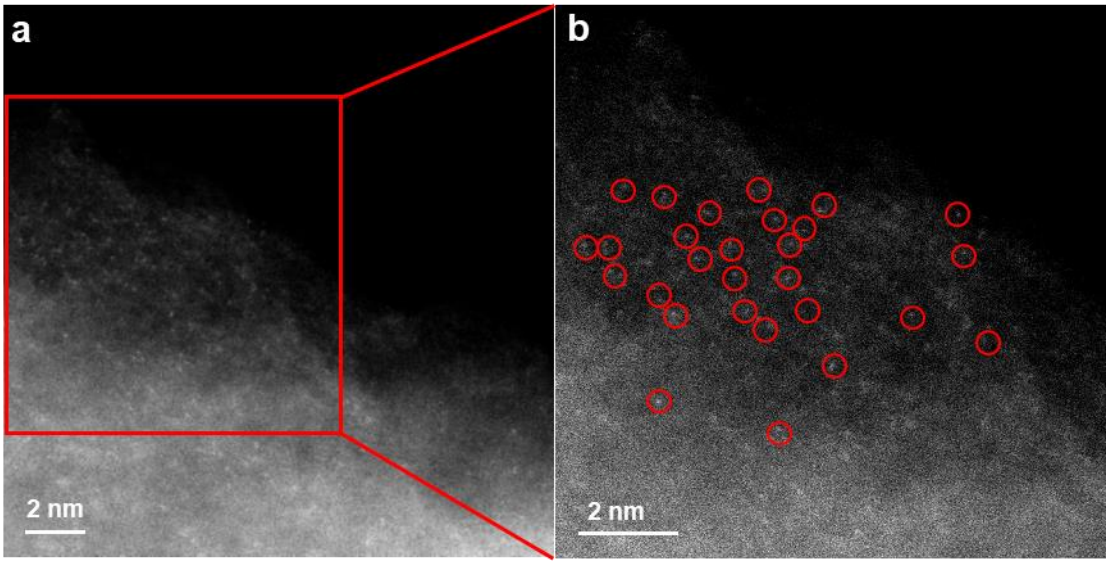

Figure S34. a HAADF-STEM and **b** magnified HAADF-STEM images of Co-SAs/NPs@NC-950 after reaction with a resolution of 2 nm. The Co nanoparticles and single atoms are marked with yellow and red circles, respectively. Single atoms and dual atoms

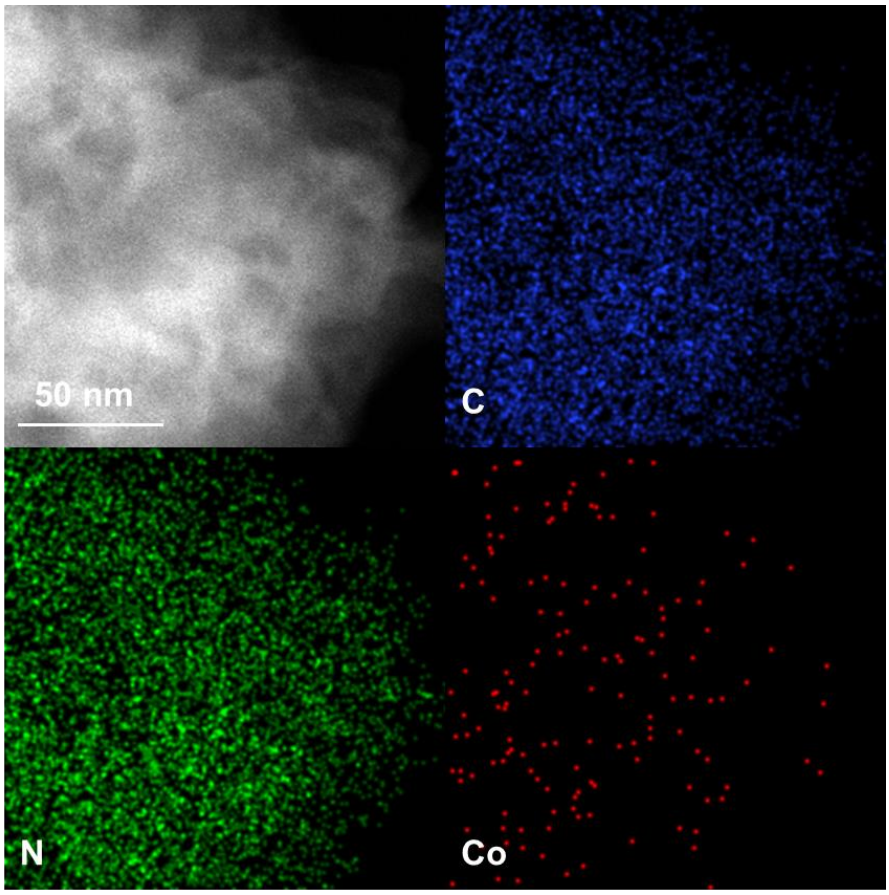

Figure S35. EDS mapping of Co-SAs/NPs@NC-950 after reaction.

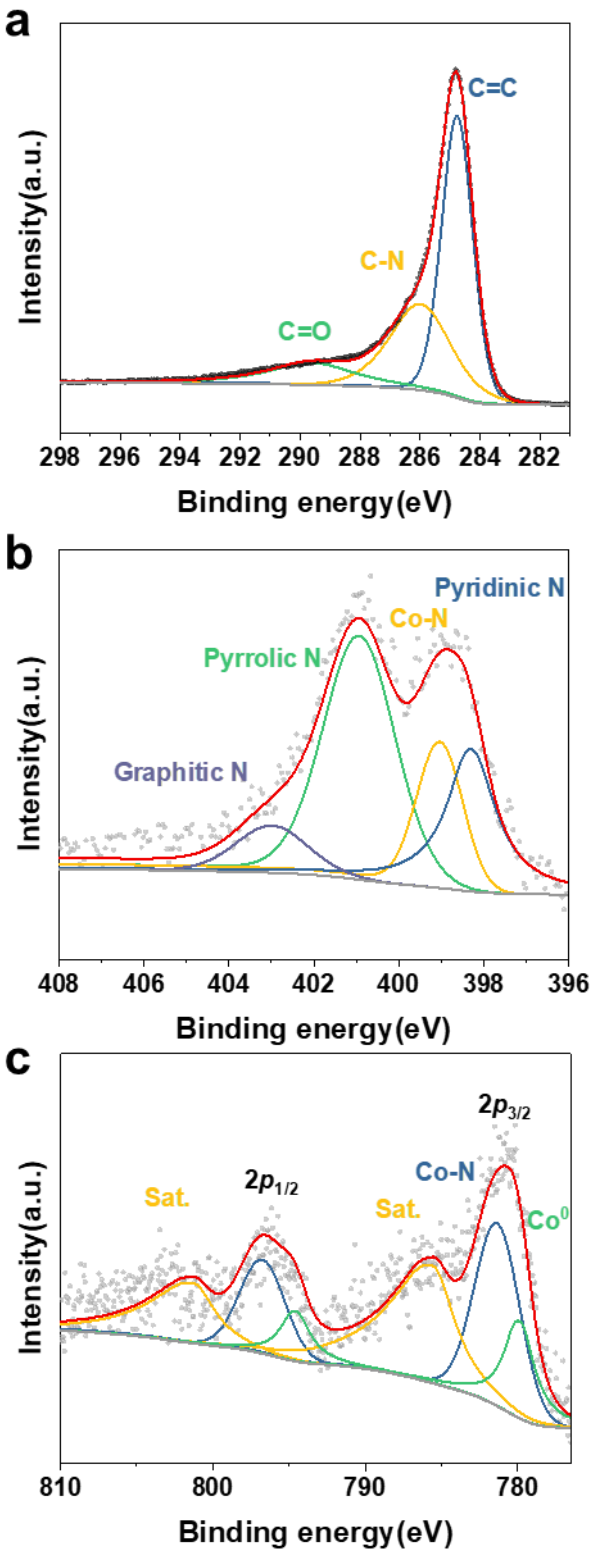

Figure S36. a C 1*s*, **b** N 1*s* and **c** Co 2*p* spectra of Co-SAs/NPs@NC-950 after the reaction.

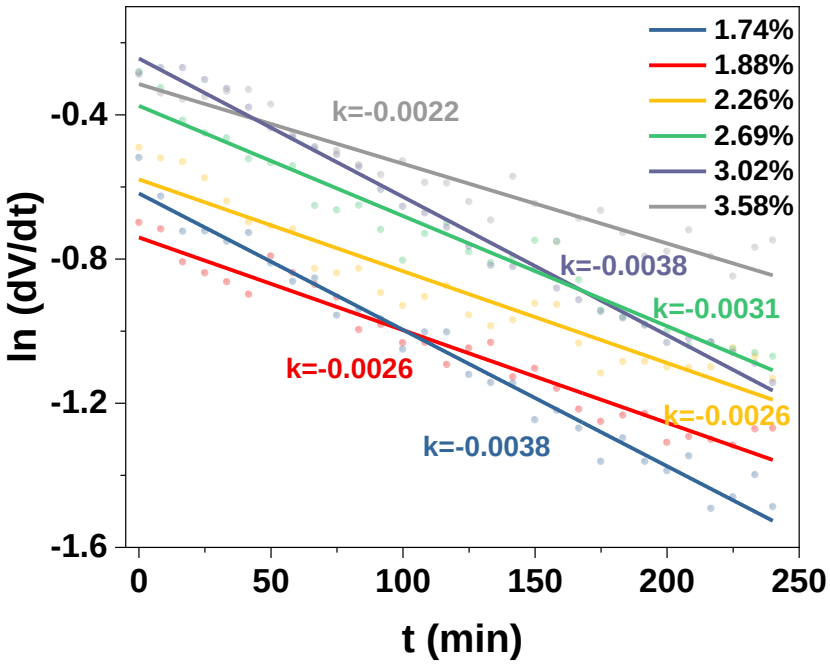

Figure S37. Kinetics of hydrogen release reaction at different cobalt contents.

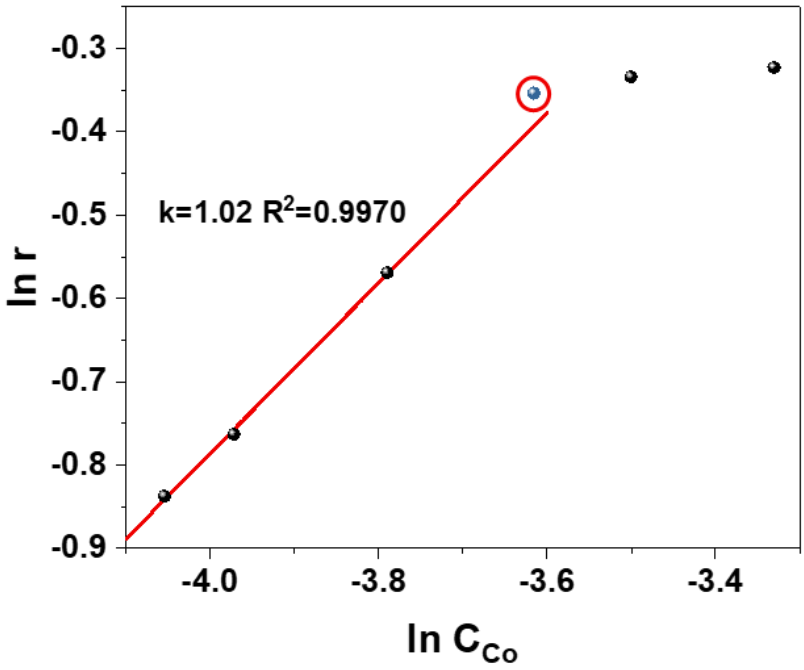

Figure S38. Kinetic reaction order to cobalt concentration during formic acid dehydrogenation over Co-SAs/NPs@NC-950 catalyst.

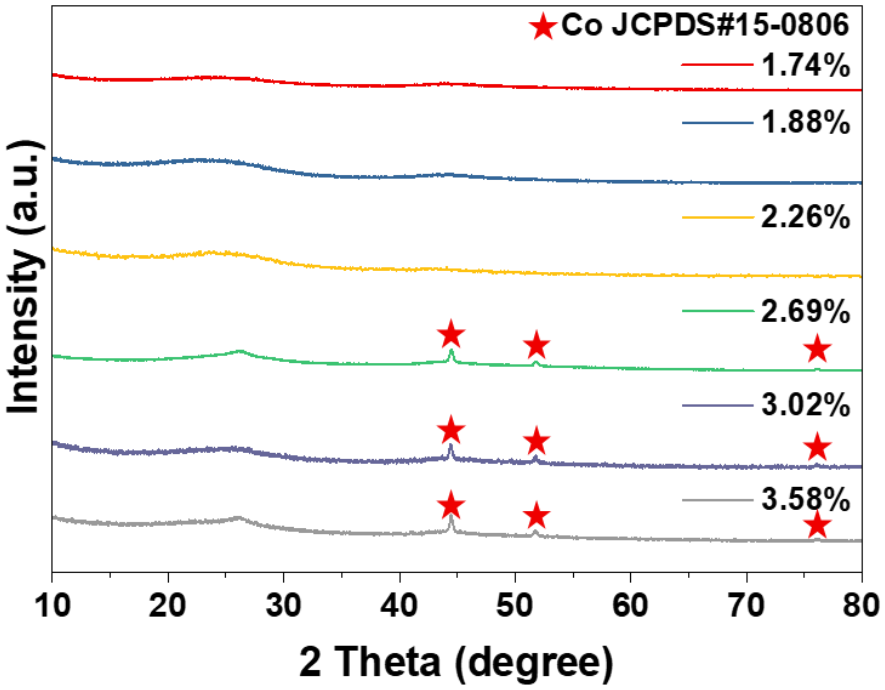

Figure S39. XRD spectra of Co-SAs/NPs@NC-950 catalyst with different cobalt contents.

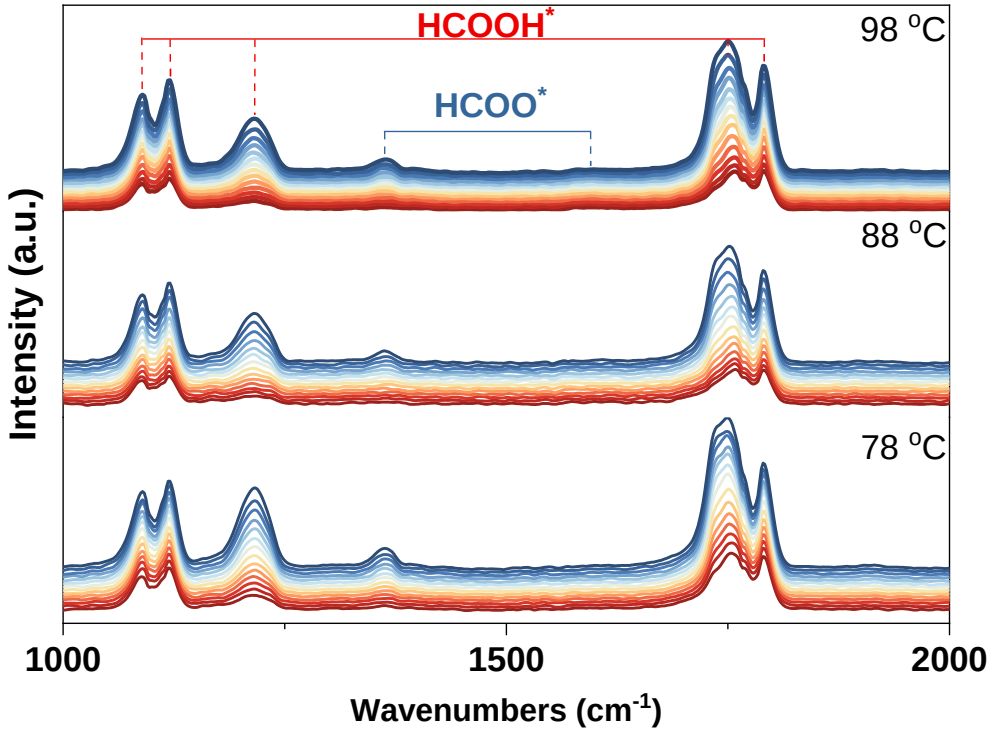

Figure S40. In-situ DRIFT spectra of HCOOH dehydrogenation over Co-SAs/NPs@NC at 98 ℃, 88 ℃ and 78 ℃.

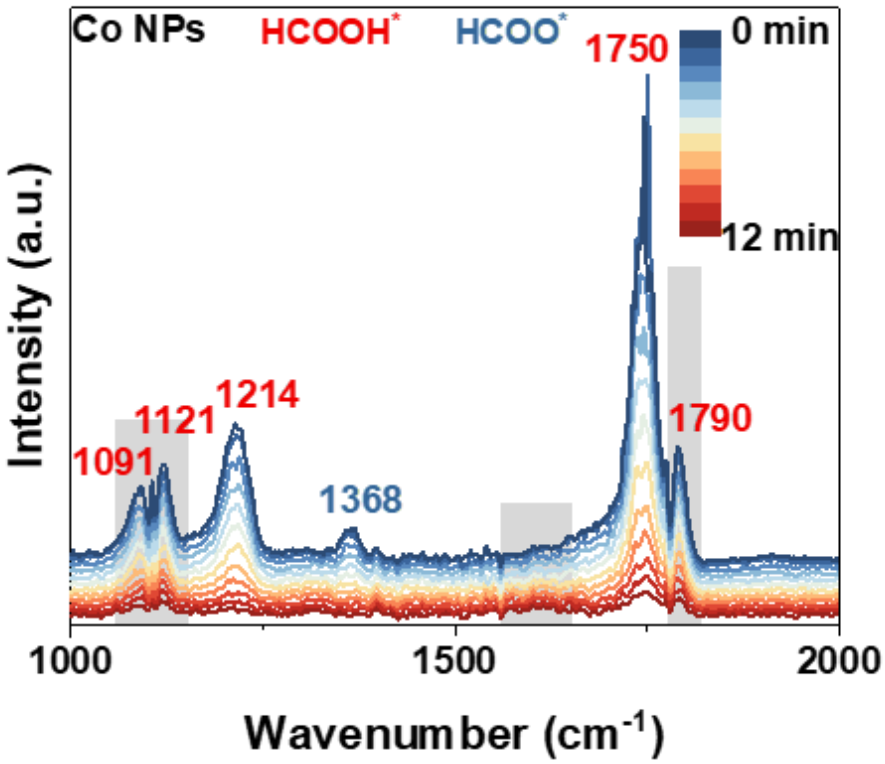

Figure S41. In-situ DRIFT spectra of HCOOH dehydrogenation over Co NPs.

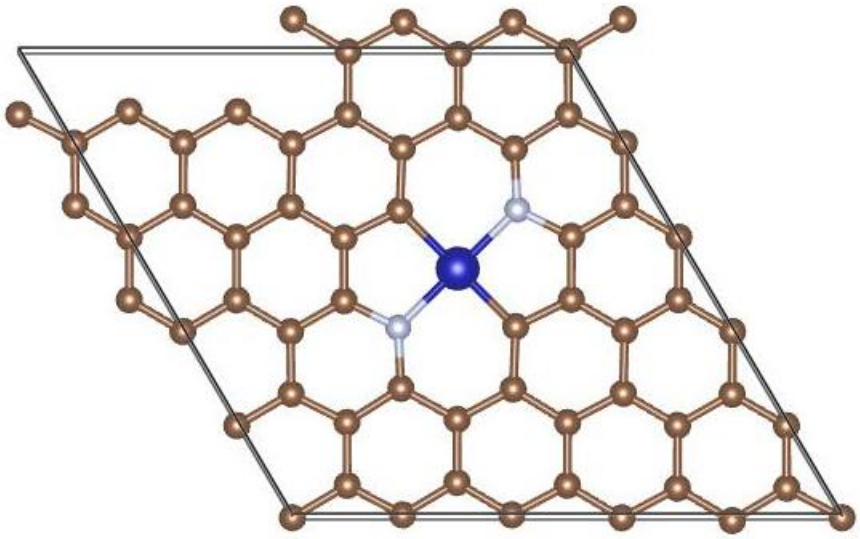

Figure S42. Lattice structure of Co SAs.

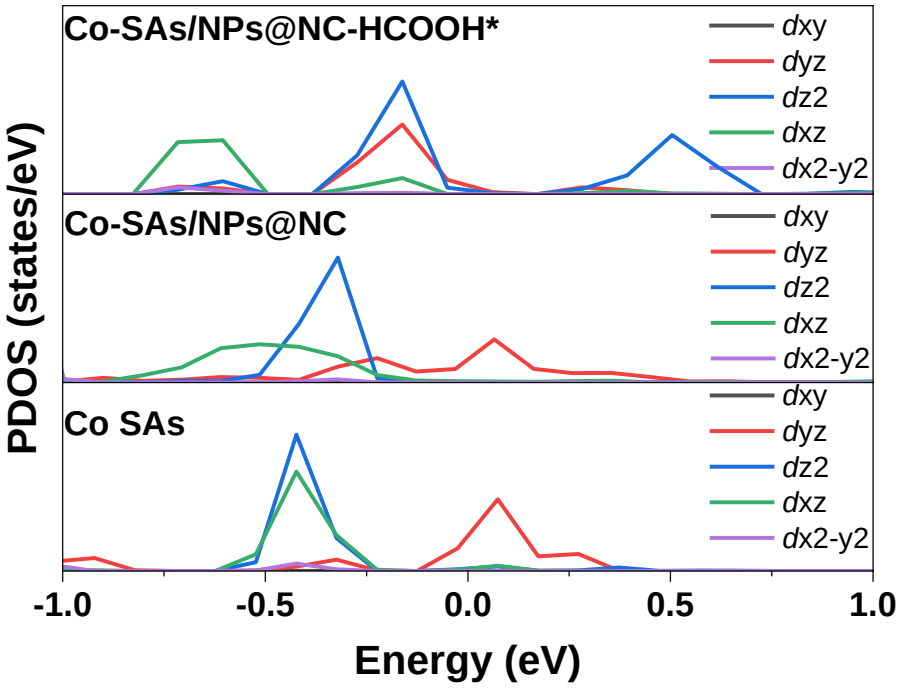

Figure S43. PDOS of Co d-orbital for Co-SAs/NPs@NC-HCOOH*, Co-SAs/NPs@NC, and Co SAs.

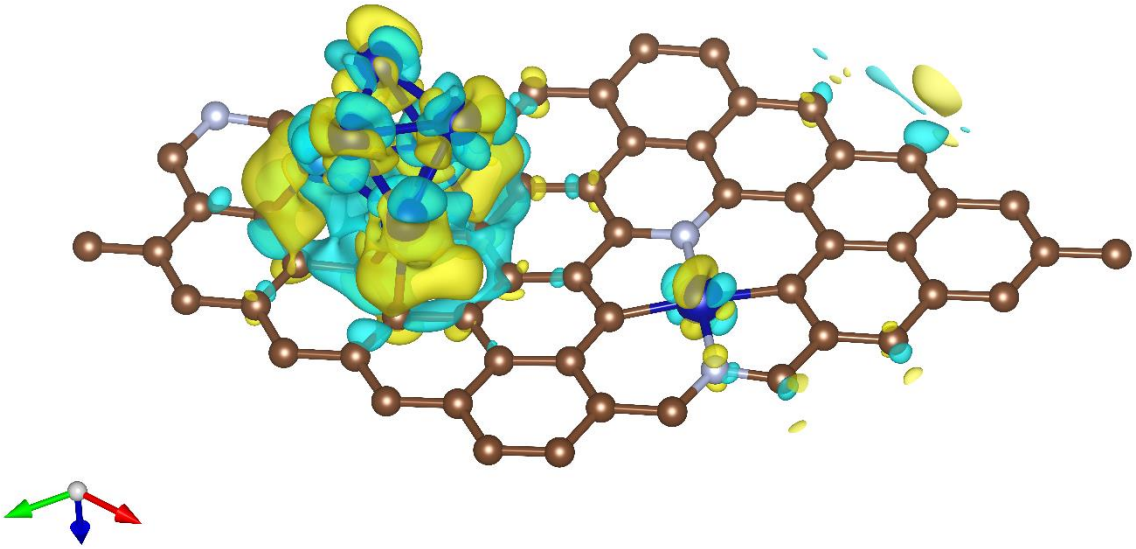

Figure S44. 3D isosurfaces of charge density differences for Co-SAs/NPs@NC.

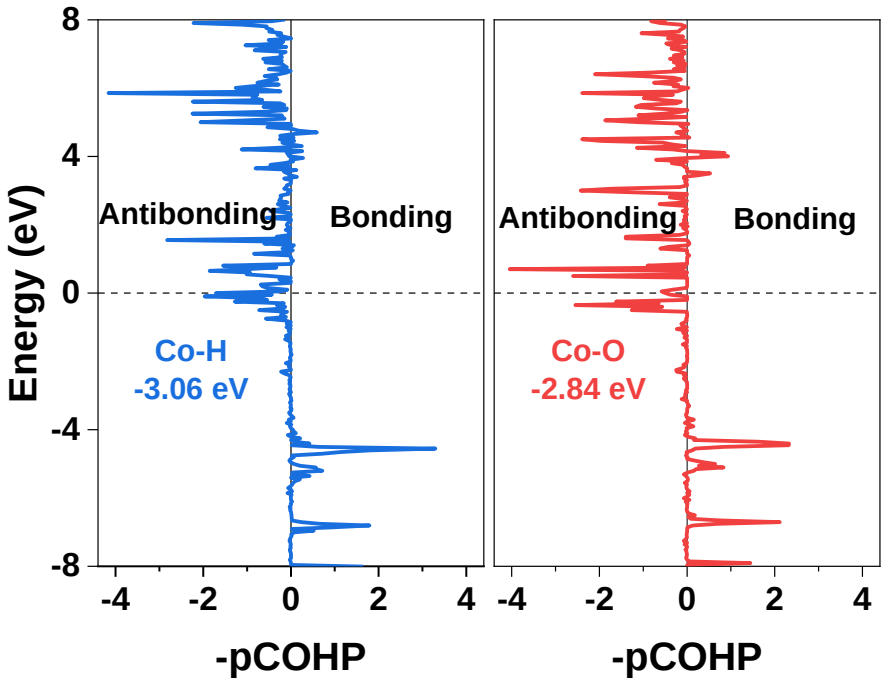

Figure S45. –pCOHP of the Co−O bond for HCOOH adsorption on Co-SAs/NPs@NC (left) and Co SAs (right).

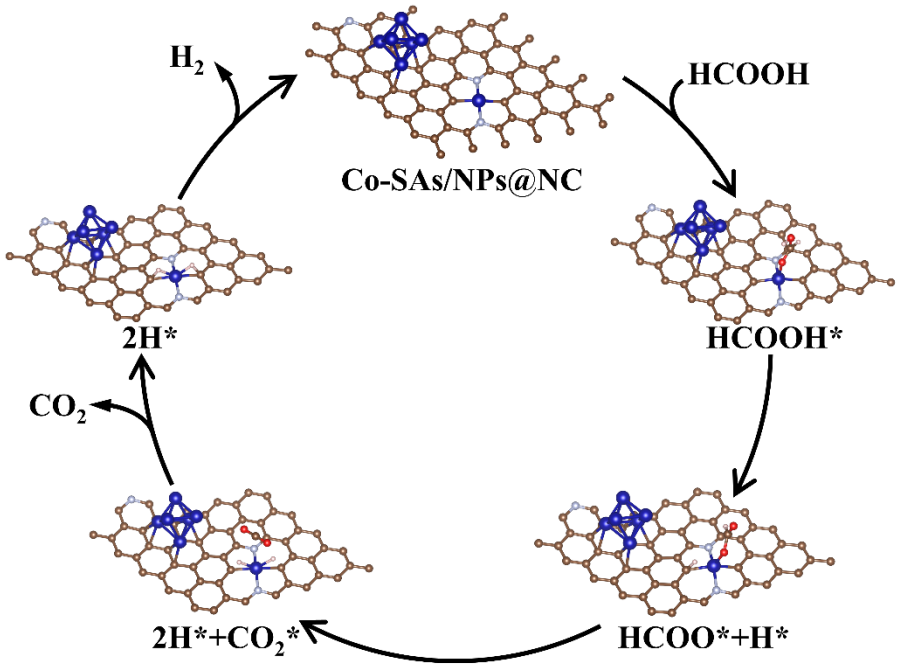

Figure S46. The selective dehydrogenation process of HCOOH on Co-SAs/NPs@NC.

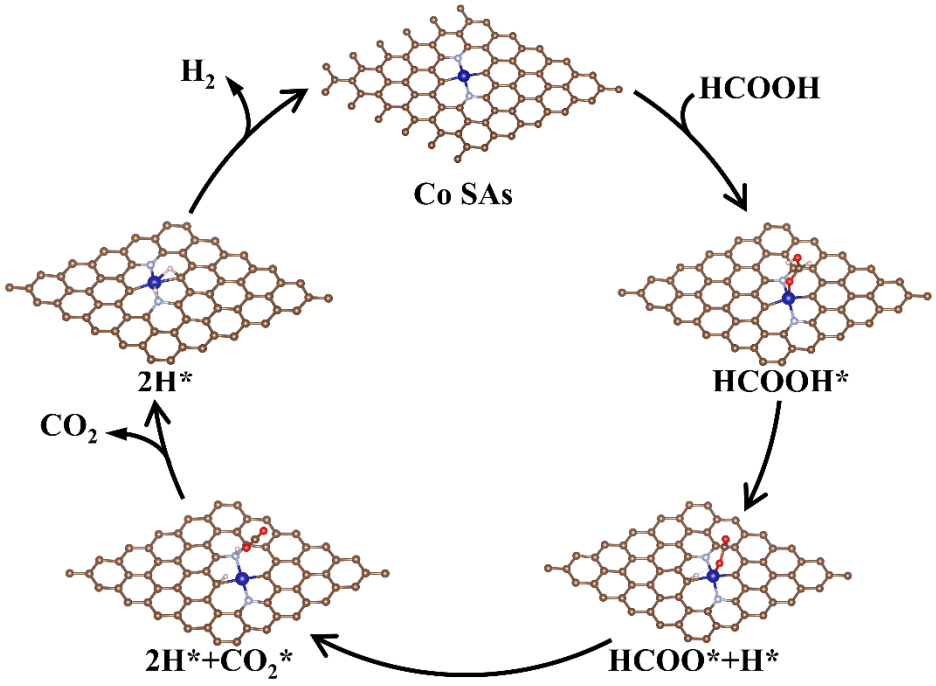

Figure S47. The selective dehydrogenation process of HCOOH on Co SAs.

5 Supplementary Tables

Table S1. Comparison of surface area and pore size of different ZIF pyrolysis materials.

Catalysts	surface area ($m^2 \cdot g^{-1}$)	pore volume ($cm^3 \cdot g^{-1}$)	Reference
N-doped carbons (C-1000)	903	0.41	2
Fe-N-aRS_{H3PO4}	977	0.88	3
ZC50	1221.5	0.58	4
OP-Fe-NC	586.5	0.11	5
Co_{NC-SA}/N*–C	298.6	0.40	6
h-CoNC	293.5	0.11	7
Co-SAs/NPs@NC-750	787	0.32	
Co-SAs/NPs@NC-850	1068	0.36	This work
Co-SAs/NPs@NC-950	**1261**	**0.37**	

Table S2. Cobalt and zinc content of the Co-SAs/NPs@NC-950, Co-SAs/NPs@NC-850 and Co-SAs/NPs@NC-750 tested by AAS

Catalysts	Co/%	Zn/%
Co-SAs/NPs@NC-750	2.73	6.37
Co-SAs/NPs@NC-850	2.74	2.68
Co-SAs/NPs@NC-950	2.69	/

Table S3. Elemental analysis of the Co-SAs/NPs@NC-950, Co-SAs/NPs@NC-850 and Co-SAs/NPs@NC-750.

Catalysts	N/%	C/%	H/%	O/%
Co-SAs/NPs@NC-750	16.53	48.47	3.01	21.75
Co-SAs/NPs@NC-850	10.42	64.71	2.43	24.14
Co-SAs/NPs@NC-950	3.36	67.79	3.00	24.61

Table S4. The atomic percentages of each substance of the Co-SAs/NPs@NC-950, Co-SAs/NPs@NC-850 and Co-SAs/NPs@NC-750.

Catalysts	C/%	N/%	O/%	Co/%	Zn/%
Co-SAs/NPs@NC-750	73.23	13.78	7.89	0.47	4.62
Co-SAs/NPs@NC-850	80.46	8.57	9.74	0.66	0.56
Co-SAs/NPs@NC-950	87.73	4.02	7.80	0.46	0

Table S5. EXAFS fitting parameters at the Co K-edge for various samples. (S_0^2=0.81)

Sample	Path	C.N.	R (Å)	$\sigma^2\times10^3$ (Å^2)	ΔE (eV)	R factor	k-space fit range	R-space fit range
Co-SAs/NPs@NC-950	Co-C	1.8±0.3	1.87±0.01	7.2±2.0	7.2±1.6	0.003	3-11	1-3
	Co-N	2.2±0.4	1.91±0.01	5.3±2.0				
	Co-Co	2.1±0.5	2.52±0.03	3.1±0.7				
Co-SAs/NPs@NC-850	Co-N	3.2±0.3	1.95±0.01	5.6±2.3	-6.6±0.8	0.005	3-11	1-3
	Co-C	0.9±0.2	2.17±0.03	6.7±2.3				
Co-SAs/NPs@NC-750	Co-N	3.8±0.3	1.87±0.02	5.0±0.4	9.0±3.1	0.011	3-11	1-3

C.N.: coordination numbers; *R*: bond distance; σ^2: Debye-Waller factors; Δ*E*: the inner potential correction. *R* factor: goodness of fit. * Fitting with fixed parameters.

Table S6. Cobalt content and gas production rate of samples with different CoZn ratios.

$Zn(NO_3)_2$/mmol	$Co(NO_3)_2$/mmol	Co/%	Gas generation rate ($mL \cdot g_{Co}^{-1} \cdot h^{-1}$)
30	0.875	1.74	518.7
30	1.75	1.88	518.4
30	2.625	2.26	520.0
30	3.5	2.69	521.9
30	7.0	3.02	474.9
30	14.0	3.58	404.7

Table S7. The atomic percentages of each substance of the Co-SAs/NPs@NC-950-1h, Co-SAs/NPs@NC-950-0.5h and Co-SAs/NPs@NC-950-2h.

Catalysts	C/%	N/%	O/%	Co/%	Zn/%
Co-SAs/NPs@NC-950-1h	87.73	4.02	7.80	0.46	0
Co-SAs/NPs@NC-950-0.5h	86.35	5.92	6.90	0.63	0.21
Co-SAs/NPs@NC-950-2h	88.71	4.54	6.21	0.54	0

Table S8. Screening of reaction conditions[a].

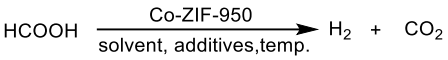

Entry	Solvent (mL)	Additive	T_{set} (°C)	Gas production volume in the initial 1 hour (mL)	Gas production rate based on Co[b] ($L \cdot g^{-1} \cdot h^{-1}$)	Gas production volume in the 4 hours[c] (mL)
1	**PC**	**No**	**110 (98)**	**42.1**	**52.2**	**123.0**
2	PC	No	90 (78)	8.4	10.4	25.1
3	PC	No	100 (88)	16.5	20.4	62.6
4	PC	No	118 (106)	56.1	69.6	207.1
5	H_2O	No	100 (88)	13.0	16.1	27.0
6	DXA	No	85 (75)	16.0	19.8	54.1
7	BAC	No	110 (98)	20.0	24.8	38.0
8	PhMe	No	110 (98)	27.2	33.7	87.6
9	Triglyme	No	110 (98)	12.0	14.9	26.5
10	CYC	No	100 (88)	32.9	40.7	115.2
11	PC	NEt_3	110 (98)	26.5	32.8	73.5
12	PC	HCOONa[d]	110 (98)	35.0	43.4	81.0
13	PhMe	HCOONa[d]	110 (98)	22.2	27.6	79.3

[a] Reaction conditions: FA (10 mmol, 377 μL), additive (1.0 mmol, 10 mol %), catalyst (30 mg) in specified solvents (6 mL). The set temperature was around 12°C higher than the actual reaction temperature shown in parentheses. [b] The rate based on gram of Co in the initial 1 hour. [c] Total gas production of H_2 and CO_2 measured for 4 h. [d] The molar ratio of FA to HCOONa in the precursors was 10. Key: propylene carbonate (PC), 1,4-dioxane (DXA), n-butyl acetate (BAC), toluene (PhMe), triglyme, cyclohexanone (CYC), triethylamine (NEt_3), and sodium formate (HCOONa).

Table S9. GC results for the Co-SAs/NPs@NC-950 catalyzed FA dehydrogenation.

	H_2 (Vol%)	CO_2 (Vol%)	CO (Vol%)	H_2 / CO_2	Time (h)
Co-SAs/NPs@NC-950/PC-110 °C	50.15	49.84	0.02	1.01	4
Co-SAs/NPs@NC-950/PC-110 °C	57.40	42.57	0.03	1.35	72
Co-SAs/NPs@NC-950/DXA -110 °C	51.06	48.92	0.02	1.04	4
Co-SAs/NPs@NC-950/BAC -110 °C	56.37	43.56	0.07	1.29	4
Co-SAs/NPs@NC-950/H_2O -110 °C	67.71	32.17	0.13	2.10	4
Co-SAs/NPs@NC-950/MB-110 °C	48.84	51.12	0.04	0.96	4
Co-SAs/NPs@NC-950/Tiglyme-110 °C	45.22	54.75	0.03	0.83	4
Co-SAs/NPs@NC-950/CYC-110 °C	53.58	46.36	0.06	1.16	4
Co-SAs/NPs@NC-950/PC-110 °C-NEt_3[a]	48.90	51.08	0.02	0.96	4
Co-SAs/NPs@NC-950/PC-110 °C-HOONa[b]	54.52	45.41	0.07	1.20	4
Co-SAs/NPs@NC-950/MB-110 °C-HOONa[b]	52.01	47.73	0.26	1.09	4

[a]NEt_3 is added with a molar ratio to HCOOH of 1 to 10. [b]HOONa is added as additive with a 10% molar ratio.

General conditions: HCOOH (10 mmol, 377 μL), 30 mg Co-SAs/NPs@NC-950, solvent (6 mL), T_{set}: 110 °C, T_{actual}: 98 °C, 4 h. Solvents include propylene carbonate (PC), 1,4-dioxane (DXA), n-butyl acetate (BAC), methyl benzene (MB), triglyme, and cyclohexanone (CYC). Volume and content of the gas phase were analyzed by manual burettes and gas chromatography (GC), respectively. Values after correction by the blank volume. All experiments were performed at least twice; average values are shown (St. Dev.<10%).

Table S10. Comparison of the apparent activation energy of different materials.

Catalysts	apparent activation energy (KJ/mol)	Reference
Pd–WOx/NPCC	87.9	8
$Pd_{0.6}Au_{0.4}$@CTF	41.2	9
Pd/C	42	10
Pd@Bi/C	44	10
$Pd_{60}Au_{40}$/HPC-NH_2	64.8	11
PdAg-MnO_x/N-SiO_2	72.4	12
Co-SAs/NPs@NC-950	**88.4**	**This work**

Table S11. Comparison of the catalytic performance of representative heterogeneous catalysts for the dehydrogenation of formic acid in the liquid phase.

Catalyst	Solvents	Temp. (°C)	Gas production rate ($mL \cdot g^{-1} \cdot h^{-1}$)	Selectivity (%)	Ref.
Co@NC-Gr2	o-xylene	95.5	62.0	99.50	13
MoS_2/Graphene[a]	/	145	83.3	/	14
5% Pd/C	PC	98	96.2	/	
5% Pt/C	PC	98	147.6	/	
Co(1)/Phen(2)/C	PC	98	158.0	/	15
Co-N-C(NPs)	PC	98	229.2	99.88	1
γ -Mo_2N/0.2NK-C	H_2O	87	293.9	≈100	16
Soybean-Mo (0.1)	H_2O	110	293.9	100	17
Co-N-C(SACs)	PC	98	319.2	99.63	1
Co(1)/Phen(7)/C	PC	98	423.3	99.80	15
Co/Cu-N-C	PC	98	1331.2	99.93	18
Pd-PCN-350R	PC	110	766	/	19
PF-$Mo_{1.98}C_{1.02}$	H_2O+Sodium formate	100	790	≈100	20
Pd-PCN-350R	toluene	120	3844	100	19
Co-SAs/NPs@NC-750	PC	98	257.7	/	
Co-SAs/NPs@NC-850	PC	98	557.3	/	
Co-SAs/NPs@NC-950	PC	98	1403.8	**99.96**	**This work**

[a] Catalytic decomposition of formic acid vapors.

Table S12. Comparison of catalytic performance for FA dehydrogenation.

Catalyst	Other reactants	Temp. (°C)	TOF (h^{-1})	Selectivity (%)	Ref.
$Ti_3C_2T_x$-250	H_2O	80	960	100	21
Co-N_4P SA sites	H_2O	80	589.5	≈100	22
Pd/Cvin. $ZnCl_2$	H_2O	50	76	100	23
Au–Pd/ED-MIL-101	H_2O+Sodium formate	90	57	100	24
$Co_{0.30}Au_{0.35}Pd_{0.35}$/C	No	25	80	100	25
Pd/N-CM (≈2.6 nm)	No	100	436	95.50	26
Co(1)/phen(7)/C	No	98	220	99.80	15
Co-N-C (SACs)	No	98	357	99.63	1
Co-SAs/NPs@NC-750	No	98	15		
Co-SAs/NPs@NC-850	No	98	46		
Co-SAs/NPs@NC-950	**No**	**98**	**83[a]**		**This work**

[a] The TOF was calculated based on the total content of single atoms and nanoparticles.

Table S13. Gas production after 5 consecutive recycling experiments.

Number of recycle reactions	Mass of remaining catalyst (mg)	Gas production volume in the initial 1 hour (mL)	Gas production rate ($mL \cdot g^{-1} \cdot h^{-1}$)
1	30.0	42.1	1403.8
2	23.0	34.9	1516.4
3	18.5	26.3	1422.8
4	16.1	22.4	1389.7
5	11.1	17.1	1541.4

General conditions: HCOOH (10 mmol, 377 μL), 30 mg Co-SAs/NPs@NC-950, PC (6 mL), T_{set}: 110 °C, T_{actual}: 98 °C, 4 h. Volume and content of the gas phase were analyzed by manual burettes and gas chromatography (GC), respectively. Values after correction by the blank volume. All experiments were performed at least twice; average values are shown (St. Dev.<10%).

General procedure:

Under an Ar atmosphere, PC (6 mL) and Co-SAs/NPs@NC-950 (30 mg) were added to a 50 mL three-neck glass reactor equipped with a magnetic stir bar. Then, the reaction solution was heated to 98 °C. After that, 10 mmol formic acid was added. The reaction was performed at the set temperature for 4 h. The generated gas was collected by a manual burette to get the gas volume. The gas was analyzed by GC. For catalyst recycling, the reaction conditions were the same as described in the original manuscript, except that the formic acid dehydrogenation reaction was repeated for five times after separating the catalyst after each reaction.

Table S14. Co loss results after different catalytic reactions.

Catalysts	Reaction time (min)	Co loss (%)
Co-SAs/NPs@NC-950	240	7.2
Co-SAs/NPs@NC-950	4320	12.7
Co SAs	240	12.8
Co SAs	4320	21.8

Table S15. Comparison between the activities of Co-SAs/NPs@NC, Co SAs and Co NPs.

Catalysts	Co (wt%)	Gas production volume in the initial 1 hour (mL)	Gas production rate ($mL \cdot g^{-1} \cdot h^{-1}$)	4h gas production (mL)
Co-SAs/NPs@NC	2.69	42.1	1403.8	123.0
Co SAs	2.21	26.0	866.8	72.2
Co NPs	9.61	36.0	1198.9	108.0

Supplementary References

1. Li X, *et al.* Cobalt single-atom catalysts with high stability for selective dehydrogenation of formic acid. *Angew. Chem. Int. Ed.* **59**, 15849-15854 (2020).
2. Chao S, *et al.* Nitrogen-doped carbon derived from ZIF-8 as a high-performance metal-free catalyst for acetylene hydrochlorination. *Sci. Rep.* **7**, 39789 (2017).
3. Patowary S, Chetry R, Goswami C, Chutia B, Bharali P. Oxygen reduction reaction catalysed by supported nanoparticles: advancements and challenges. *ChemCatChem.* **14**, e202101472 (2022).
4. Qiu J, *et al.* Size-controllable synthesis of ZIF-8 and derived nitrogen-rich porous carbon for CO_2 and VOCs adsorption. *ChemistrySelect* **7**, e202203273 (2022).
5. Li J, *et al.* Selective etching of metal-organic frameworks for open porous structures: mass-efficient catalysts with enhanced oxygen reduction reaction for fuel cells. *J. Am. Chem. Soc.* **145**, 27262-27272 (2023).
6. Wang M, *et al.* Interfacial water activation by single-atom Co–N_3 sites coupled with encapsulated Co nanocrystals for accelerating electrocatalytic hydrogen Evolution. *ACS Catal.* **12**, 10771-10780 (2022).
7. Han X, *et al.* Hollow mesoporous atomically dispersed metal-nitrogen-carbon catalysts with enhanced diffusion for catalysis involving larger molecules. *Nat. Commun.* **13**, 2900 (2022).
8. Zhang A, Xia J, Yao Q, Lu Z H. Pd-WO_x heterostructures immobilized by MOFs-derived carbon cage for formic acid dehydrogenation. *Appl. Catal. B* **309**, 121278 (2022).
9. Wang J, *et al.* Covalent triazine framework encapsulated ultrafine PdAu alloy nanoclusters as additive-free catalysts for efficient hydrogen production from formic acid. *ACS Catal.* **13**, 5135-5146 (2023).
10. Qin X, *et al.* Mechanistic analysis-guided Pd-based catalysts for efficient hydrogen production from formic acid dehydrogenation. *ACS Catal.* **10**, 3921-3932 (2020).
11. Wang Z, *et al.* Ultrasmall PdAu alloy nanoparticles anchored on amine-functionalized hierarchically porous carbon as additive-free catalysts for highly efficient dehydrogenation of formic acid. *Appl. Catal. B* **291**, 120140 (2021).

12. Bulut A, *et al.* MnO_x-Promoted PdAg alloy nanoparticles for the additive-free dehydrogenation of formic acid at room temperature. *ACS Catal.* **5**, 6099-6110 (2015).

13. Chernov AN, Astrakova TV, Sobolev VI, Koltunov KY. Liquid versus gas phase dehydrogenation of formic acid over Co@N-doped carbon materials. The role of single atomic sites. *Mol. Catal.* **504**, 111457 (2021).

14. Koroteev VO, Bulushev DA, Chuvilin AL, Okotrub AV, Bulusheva LG. Nanometer-sized MoS_2 clusters on graphene flakes for catalytic formic acid decomposition. *ACS Catal.* **4**, 3950-3956 (2014).

15. Tang C, *et al.* A stable nanocobalt catalyst with highly dispersed CoN_x active sites for the selective dehydrogenation of formic acid. *Angew. Chem. Int. Ed.* **56**, 16616-16620 (2017).

16. Yu Z, *et al.* Selective dehydrogenation of aqueous formic acid over multifunctional γ-Mo_2N catalysts at a temperature lower than 100 ^oC. *Appl. Catal. B* **313**, 121445 (2022).

17. Wang J, *et al.* Non-precious molybdenum-based catalyst derived from biomass: CO-free hydrogen production from formic acid at low temperature. *Energy Convers Manage* **164**, 122-131 (2018).

18. Shi Y, *et al.* Atomically dispersed cobalt/copper dual-metal catalysts for synergistically boosting hydrogen generation from formic acid. *Angew. Chem. Int. Ed.* **62**, e202313099 (2023).

19. Chen Z, *et al.* Designing a robust palladium catalyst for formic acid dehydrogenation. *ACS Catal.* **13**, 4835-4841 (2023).

20. Lv C, *et al.* Efficient hydrogen production via sunlight-driven thermal formic acid decomposition over a porous film of molybdenum carbide. J. Mater. Chem. A **9**, 22481-22488 (2021).

21. Hou T, *et al.* Modulating oxygen coverage of $Ti_3C_2T_x$ MXenes to boost catalytic activity for HCOOH dehydrogenation. *Nat. Commun.* **11**, 4251 (2020).

22. Liu H, *et al.* Asymmetric coordination of single-atom Co sites achieves efficient dehydrogenation catalysis. *Adv. Funct. Mater.* **32**, 2207408 (2022).

23. Santos JL, Megías-Sayago C, Ivanova S, Centeno MÁ, Odriozola JA. Functionalized biochars as supports for Pd/C catalysts for efficient hydrogen production from formic acid. *Appl. Catal. B* **282**, 119615 (2021).

24. Gu X, Lu Z, Jiang H, Akita T, Xu Q. Synergistic catalysis of metal-organic framework-immobilized Au–Pd nanoparticles in dehydrogenation of formic acid for chemical hydrogen storage. *J. Am. Chem. Soc.* **133**, 11822-11825 (2011).

25. Wang Z, et al. An efficient CoAuPd/C catalyst for hydrogen generation from formic acid at room temperature. *Angew. Chem. Int. Ed.* **52**, 4406-4409 (2013).

26. Bulushev DA, *et al.* Single isolated Pd^{2+} cations supported on N-doped carbon as active sites for hydrogen production from formic acid decomposition. *ACS Catal.* **6**, 681-691 (2016).